

cy. 4

NOV 2 1976

APR 28 1982

DEC 15 1983



ANALYTICAL MODEL OF SUPERSONIC, TURBULENT, NEAR-WAKE FLOWS

ENGINE TEST FACILITY
ARNOLD ENGINEERING DEVELOPMENT CENTER
AIR FORCE SYSTEMS COMMAND
ARNOLD AIR FORCE STATION, TENNESSEE 37389

September 1976

Final Report for Period July 1973 — December 1975

Approved for public release; distribution unlimited.

TECHNICAL REPORTS
FILE COPY

Prepared for

DIRECTORATE OF TECHNOLOGY (DYR)
ARNOLD ENGINEERING DEVELOPMENT CENTER
ARNOLD AIR FORCE STATION, TENNESSEE 37389

Property of U. S. Air Force

PROPERTY OF U. S. AIR FORCE
AEDC TECHNICAL LIBRARY
ARNOLD AFB, TN 37389

PROPERTY OF U. S. AIR FORCE
AEDC TECHNICAL LIBRARY
ARNOLD AFB, TN 37389

NOTICES

When U. S. Government drawings specifications, or other data are used for any purpose other than a definitely related Government procurement operation, the Government thereby incurs no responsibility nor any obligation whatsoever, and the fact that the Government may have formulated, furnished, or in any way supplied the said drawings, specifications, or other data, is not to be regarded by implication or otherwise, or in any manner licensing the holder or any other person or corporation, or conveying any rights or permission to manufacture, use, or sell any patented invention that may in any way be related thereto.

Qualified users may obtain copies of this report from the Defense Documentation Center.

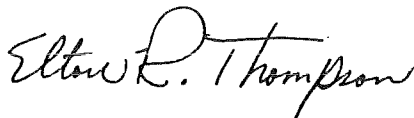
References to named commercial products in this report are not to be considered in any sense as an endorsement of the product by the United States Air Force or the Government.

This report has been reviewed by the Information Office (OI) and is releasable to the National Technical Information Service (NTIS). At NTIS, it will be available to the general public, including foreign nations.

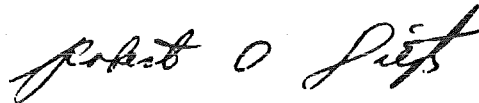
APPROVAL STATEMENT

This technical report has been reviewed and is approved for publication.

FOR THE COMMANDER



ELTON R. THOMPSON
Research & Development
Division
Directorate of Technology



ROBERT O. DIETZ
Director of Technology

UNCLASSIFIED

REPORT DOCUMENTATION PAGE		READ INSTRUCTIONS BEFORE COMPLETING FORM
1. REPORT NUMBER AEDC-TR-76-127	2. GOVT ACCESSION NO.	3. RECIPIENT'S CATALOG NUMBER
4. TITLE (and Subtitle) ANALYTICAL MODEL OF SUPERSONIC, TURBULENT, NEAR-WAKE FLOWS		5. TYPE OF REPORT & PERIOD COVERED Final Report - July 1973 - December 1975
		6. PERFORMING ORG. REPORT NUMBER
7. AUTHOR(s) C. E. Peters and W. J. Phares, ARO, Inc.		8. CONTRACT OR GRANT NUMBER(s)
9. PERFORMING ORGANIZATION NAME AND ADDRESS Arnold Engineering Development Center (DY) Air Force Systems Command Arnold Air Force Station, Tennessee 37389		10. PROGRAM ELEMENT, PROJECT, TASK AREA & WORK UNIT NUMBERS Program Element 65807F
11. CONTROLLING OFFICE NAME AND ADDRESS Arnold Engineering Development Center (DYFS), Air Force Systems Command Arnold Air Force Station, Tennessee 37389		12. REPORT DATE September 1976
		13. NUMBER OF PAGES 74
14. MONITORING AGENCY NAME & ADDRESS (if different from Controlling Office)		15. SECURITY CLASS. (of this report) UNCLASSIFIED
		15a. DECLASSIFICATION/DOWNGRADING SCHEDULE N/A
16. DISTRIBUTION STATEMENT (of this Report) Approved for public release; distribution unlimited.		
17. DISTRIBUTION STATEMENT (of the abstract entered in Block 20, if different from Report)		
18. SUPPLEMENTARY NOTES Available in DDC		
19. KEY WORDS (Continue on reverse side if necessary and identify by block number) <div style="display: flex; justify-content: space-between;"> <div> mathematical model supersonic turbulent flow flows (near-wake) </div> <div> boundary layer free stream Mach number base pressure </div> <div> transport properties turbulence interactions viscous flow </div> </div>		
20. ABSTRACT (Continue on reverse side if necessary and identify by block number) <p>An analytical model for planar and axisymmetric, supersonic, turbulent, near-wake flows is presented. The viscous region behind the blunt base is described by the integral form of the boundary-layer equations, and the inviscid outer-flow region, including the remnant of the initial turbulent boundary layer, is computed with the rotational method of characteristics. The solution of the two regions is fully coupled. A saddle-point</p>		

UNCLASSIFIED

UNCLASSIFIED

20. ABSTRACT (Continued)

singularity, similar to the Crocco-Lees critical point, occurs downstream of the rear stagnation point. The base pressure is obtained by iteration of the initial conditions until the flow-field solution will pass through the singularity. Base bleed of a gas different from the outer-stream gas is included in the formulation, and provision is made to treat equilibrium chemical reactions in the viscous wake. However, an unresolved problem has been encountered in the solution of the species conservation equations. Therefore, results for only single gas flows are presented. The analytical model is shown to adequately predict the effect of free-stream Mach number and initial boundary layer on the planar base pressure. In addition, the planar flow-field structure is well predicted. Axisymmetric base pressure and flow-field structure are reasonably well predicted for free-stream Mach numbers greater than 2.0, but the turbulent transport model used yields only fair results for Mach numbers less than 1.7. The effect of base bleed on the axisymmetric base pressure is well predicted.

UNCLASSIFIED

PREFACE

The work reported herein was conducted by the Arnold Engineering Development Center (AEDC), Air Force Systems Command (AFSC). The results were obtained by ARO, Inc. (a subsidiary of Sverdrup & Parcel and Associates, Inc.), contract operator of AEDC, AFSC, Arnold Air Force Station, Tennessee. The Program Element number was 65807F. The work was done under ARO Project Nos. RF423, R33P-60A, and R33A-02A. The authors of this report were C. E. Peters and W. J. Phares, ARO, Inc. The manuscript (ARO Control No. ARO-ETF-TR-76-69) was submitted for publication on July 1, 1976.

CONTENTS

	<u>Page</u>
1.0 INTRODUCTION	
1.1 Problem Definition	7
1.2 Review of Earlier Analytical Work	11
1.3 Important Features of a Realistic Analytical Model	15
2.0 DEVELOPMENT OF ANALYTICAL MODELS	
2.1 Basic Assumptions	16
2.2 Basic Equations	18
2.3 Shear Layer Profiles	20
2.4 Computation of Density in the Viscous Flow	21
2.5 Turbulent Transport Terms	21
2.6 Transformation of the Integral Equations	22
2.7 Solution of the Outer Flow and Coupling with the Viscous Layer	23
2.8 Expansion of the Initial Boundary Layer	24
2.9 Characterization of the Initial and Boundary Conditions	26
2.10 Two-Layer Treatment of the Outer Flow	28
2.11 Method of Solution	28
2.12 Model for the Turbulent Reynolds Number	31
3.0 DISCUSSION OF RESULTS	
3.1 Concentration Field Solution Problems	38
3.2 Planar Base Pressure	38
3.3 Planar Flow-Field Structure	42
3.4 Axisymmetric Base Pressure	48
3.5 Effect of Base Bleed on Axisymmetric Base Pressure	50
3.6 Axisymmetric Flow-Field Structure	51
3.7 Dividing Streamline Properties	57
4.0 CONCLUDING REMARKS	59
REFERENCES	60

ILLUSTRATIONS

Figure

1. Features of the Near-Wake Flow Field	8
2. Examples of Supersonic Near-Wake Flows	10
3. Nomenclature for Near-Wake Analysis	16
4. Coupling of the Shear Layer and Outer-Flow Solutions	24

<u>Figure</u>	<u>Page</u>
5. Corner Expansion of the Initial Boundary Layer	25
6. Boundary-Layer Profile Exponent for Adiabatic Flow along a Flat Plate	27
7. Boundary-Layer Momentum Thickness Ratio for Adiabatic Flow along a Flat Plate	27
8. Two-Layer Treatment of the Supersonic Flow Field	28
9. Subcritical and Supercritical Solutions	29
10. Turbulent Reynolds Number for Planar Shear Layers with No Secondary Flow	32
11. Configurations for Low-Speed Separating and Reattaching Flow Experiments	33
12. Turbulent Reynolds Number Distribution Upstream of the RSP in the Reattachment Regime	34
13. Turbulent Reynolds Number Downstream of the RSP	35
14. Influence of the Turbulent Reynolds Number at the RSP on the Predicted Base Pressure	36
15. Turbulent Reynolds Number at the RSP as a Function of the Pressure Gradient Parameter	37
16. Effect of the Initial Boundary Layer on the Base Pressure in Planar Flow ($M_{a1} = 1.5$)	39
17. Effect of the Initial Boundary Layer on the Base Pressure in Planar Flow ($M_{a1} = 2.0$)	40
18. Effect of the Initial Boundary Layer on the Base Pressure in Planar Flow ($M_{a1} = 3.0$)	40
19. Mach Number Effect on the Base Pressure for Planar Flow	41
20. Predicted Base Pressure for Planar Flow	42
21. Total Pressure at the Edge of the Shear Layer for Planar Flow	43
22. Centerline Pressure Distribution for Planar Wake Flow ($M_{a1} = 2.0$)	44
23. Centerline Pressure Distribution for Planar Wake Flow ($M_{a1} = 3.05$)	45
24. Centerline Mach Number Distribution for Planar Wake Flow ($M_{a1} = 3.05$)	46
25. Pitot Pressure Profiles for Planar Wake Flow ($M_{a1} = 3.05$)	47
26. Effect of the Initial Boundary Layer on the Base Pressure in Axisymmetric Flow ($M_{a1} = 2.0$)	48

<u>Figure</u>	<u>Page</u>
27. Effect of the Initial Boundary Layer on the Base Pressure in Axisymmetric Flow ($M_{a1} = 3.9$)	49
28. Mach Number Effect on the Base Pressure for Axisymmetric Flow	50
29. Effect of Base Bleed on Axisymmetric Base Pressure	51
30. Total Pressure at the Edge of the Shear Layer for Axisymmetric Flow	52
31. Centerline Pressure Distribution for Axisymmetric Wake Flow ($M_{a1} = 3.91$)	53
32. Pitot Pressure Profiles for Axisymmetric Wake Flow ($M_{a1} = 3.91$)	54
33. Centerline Pressure Distribution for Axisymmetric Wake Flow ($M_{a1} = 1.92$)	55
34. Centerline Mach Number Distribution for Axisymmetric Wake Flow ($M_{a1} = 1.92$)	56
35. Centerline Pressure Distribution for Axisymmetric Wake Flow ($M_{a1} = 2.03$)	57
36. Total Pressure along the Dividing Streamline for Planar Flows	58
37. Total Pressure along the Dividing Streamline for Axisymmetric Flows	59

APPENDIX

A. COEFFICIENTS OF THE INTEGRAL EQUATIONS	65
NOMENCLATURE	72

1.0 INTRODUCTION

1.1 PROBLEM DEFINITION

Turbulent near wakes behind blunt bases in supersonic external flow occur in a variety of flows of practical interest. The near-wake flow process (Fig. 1) is characterized by a strong interaction between the inviscid external flow and the turbulent portion of the flow; therefore, computation of the entire flow field requires a coupled solution for the viscous and inviscid regions.

Several features of the near-wake flow field are shown in Fig. 1. First, a recirculation region exists just downstream of the base. With no bleed flow from the base, the velocity on the centerline is zero at the base plane. When flow is bled into the base, the onset of recirculation is delayed until the bleed flow has been entrained into the turbulent shear layer. If the bleed flow is sufficiently large, the recirculation region can be eliminated. As shown in Fig. 1, the pressure just downstream of the base is considerably lower than the pressure on the body surface upstream of the base. The centerline static pressure rises slightly with distance until the bleed flow is completely entrained, then tends to decrease slightly with distance as the recirculation velocities become larger. At some distance downstream of the base, the shear layer merges with the axis and the flow begins to recompress. The recompression region is characterized by large pressure gradients and by acceleration of the flow along the centerline. Downstream of the rear stagnation point (RSP) the velocities throughout the viscous layer are positive.

If the flow is planar, and if the external flow upstream of the base is effectively infinite and parallel to the centerline, then the centerline static pressure in the recompression region monotonically rises to the free-stream static pressure. However, in an axisymmetric flow, the pressure in the recompression region "overshoots" the free-stream pressure (Fig. 1). Downstream of the recompression region the flow relaxes toward a self preserving turbulent far-wake structure, in which static pressure gradients are negligible.

Experience has shown that the base pressure and the near-wake flow structure are dependent upon (1) the thickness and shape of the boundary-layer velocity profile just upstream of the base, (2) the inviscid external flow properties (Mach number, flow angle, etc.) at the base plane, and (3) the gas properties and flow rate of the base bleed. The near-wake flow structure also depends on the lateral extent of the supersonic external flow. If the external flow is bounded by a solid wall or by a free boundary, then waves which are generated by the expansion process at the base plane will be reflected from the boundary. These reflected waves can influence the near-wake structure if they intersect the viscous wake upstream of the point where the flow on the axis has reaccelerated to supersonic speed.

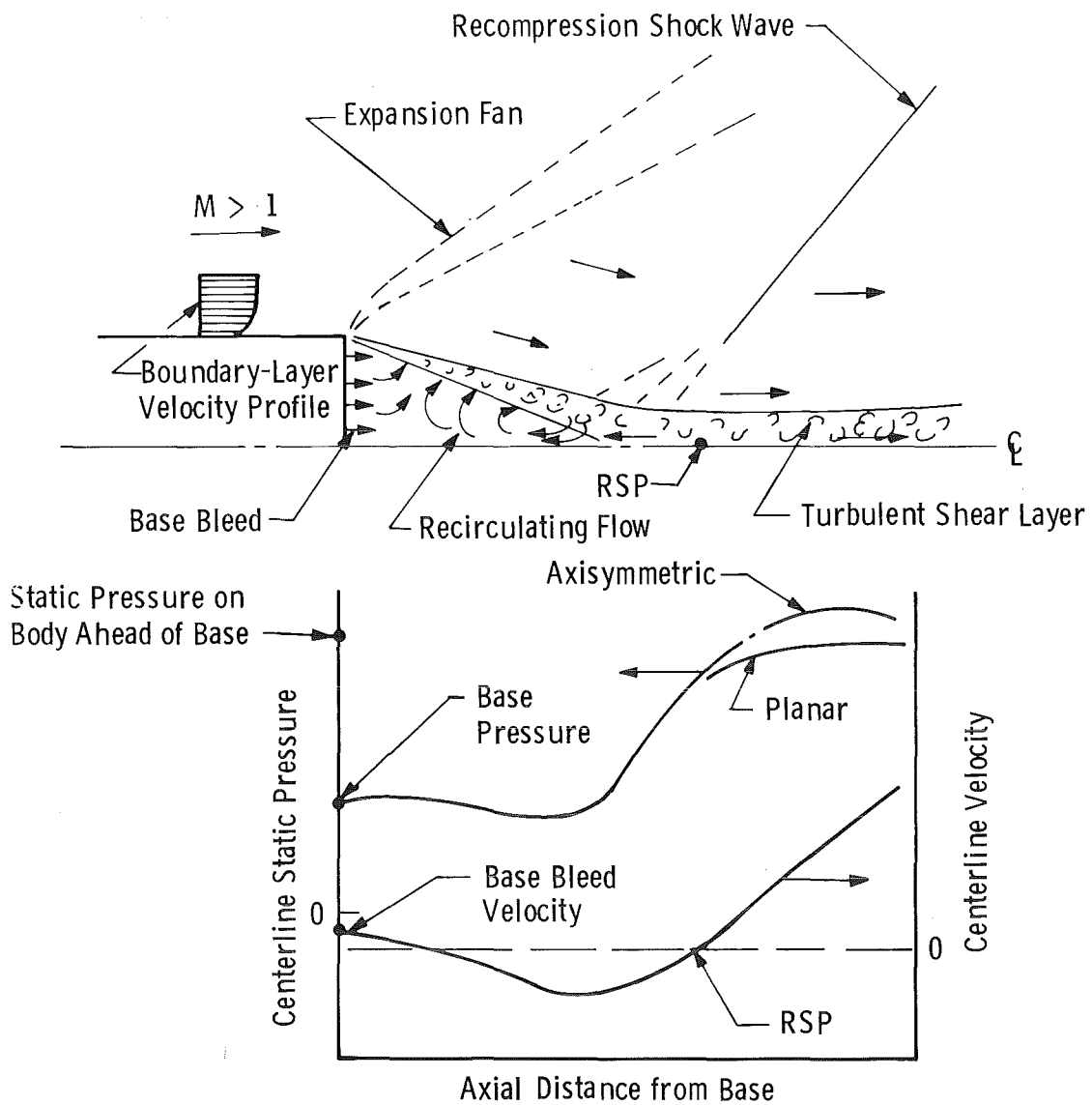


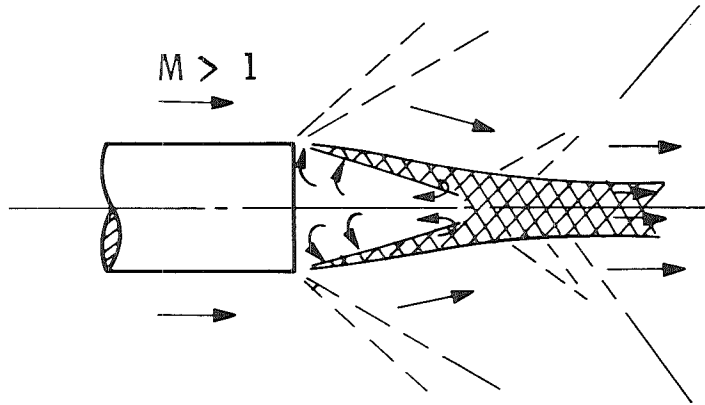
Figure 1. Features of the near-wake flow field.

Several examples of supersonic near-wake flows which are of interest at the AEDC are shown in Fig. 2. The classic turbulent near-wake flow is that behind bodies in supersonic flight (Fig. 2a). Truncated plug exhaust nozzles (Fig. 2b) have been used for both turbine engines and rockets. An accurate prediction of the plug base pressure is required for the analytical assessment of the thrust performance of such nozzles. The supersonic external flow is limited in lateral extent, and wave reflections from the free boundary must be taken into account in the prediction of the near-wake structure. Truncated plug nozzles are often operated with base bleed.

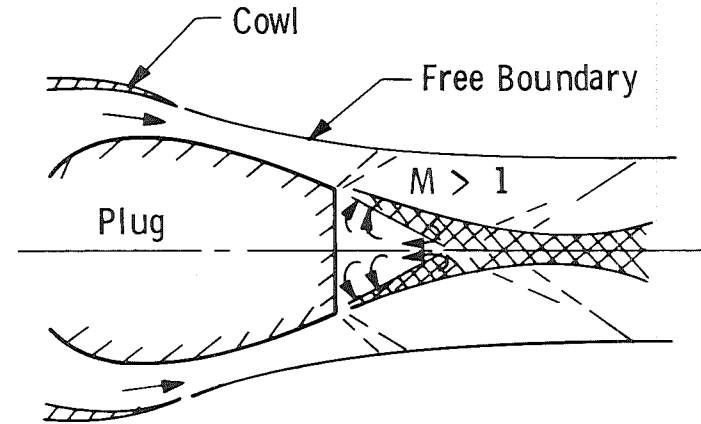
The annular ejector (Fig. 2c) is often used in place of the traditional ejector, which has a centrally located supersonic driving nozzle. The supersonic external flow in the annular ejector is bounded by a solid wall, and wave reflections from the boundary strongly interact with the near-wake structure.

A highly complex near-wake flow structure is involved with the external burning propulsion concept (Fig. 2d) which was first proposed by Strahle (Ref. 1). According to Strahle, waves are generated by the mixing and combustion process; these waves interact with the near wake and cause the base pressure to be much higher than that with no fuel injection. Indeed, Strahle suggests that the base pressure can be increased to a level greater than free-stream static pressure, perhaps to a level where net thrust can be obtained with a slender forebody. This external burning propulsion concept has been the subject of several experimental investigations (e.g., Ref. 2). It is clear that an adequate analysis of this complex flow must be based on a physically perceptive analysis of the simpler flow shown in Fig. 2a.

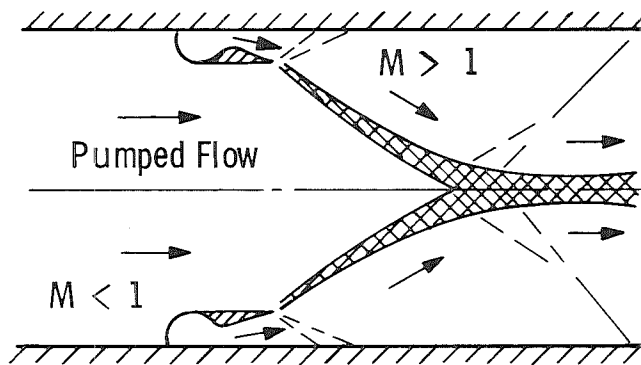
In view of the numerous practical flows in which supersonic near-wake mechanisms occur, it was decided that a generalized analysis for such flows was needed at the AEDC. The generalized analysis should include the following factors: (1) arbitrary turbulent initial boundary layers; (2) arbitrary inviscid external flow profiles at the base plane; (3) external flows which are bounded by a solid wall or by a constant pressure boundary; (4) arbitrary base bleed, including gases which can react chemically with the external flow; and (5) planar or axisymmetric geometry. The analysis should provide reasonably accurate predictions not only of the gross features of the flow, such as the base pressure, but also of the detailed flow structure in the viscous wake and in the adjacent inviscid flow field.



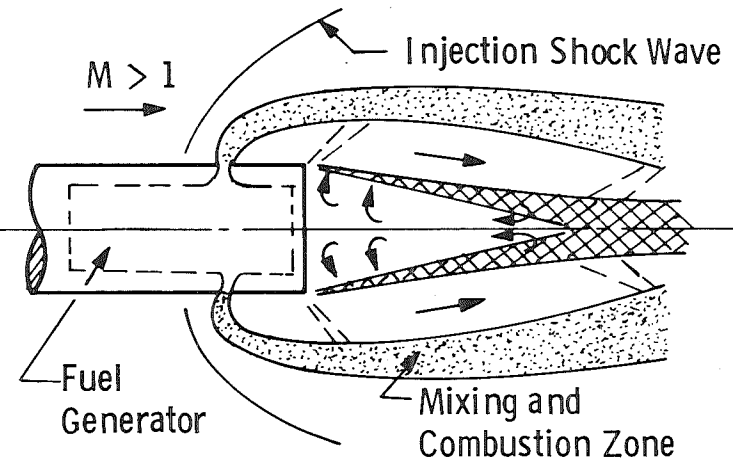
a. Bodies in supersonic flight



b. Truncated plug nozzles



c. Annular ejectors



d. External burning propulsion

Figure 2. Examples of supersonic near-wake flows.

1.2 REVIEW OF EARLIER ANALYTICAL WORK

The analysis of turbulent near-wake flows has received much attention during the past twenty-five years. Most of the work has been based either on the viscous interaction model proposed by Crocco and Lees (Ref. 3) or on the component model first developed by Korst for turbulent flows (Refs. 4 and 5). Most investigators have concentrated on planar flows, which are inherently simpler than axisymmetric flows.

Crocco-Lees Model - This integral method is based on solving the integral form of the boundary-layer equations for the viscous portion of the flow, including the reversed flow region. The planar external flow field is coupled to the viscous region by the use of the Prandtl-Meyer equations, which relate the local static pressure to the flow angle at the edge of the viscous layer. The viscous layer growth rate is computed with an empirical entrainment coefficient. A major problem in the original Crocco-Lees analysis is establishing the relationship of the integral parameters of the viscous flow profiles to the other variables of the problem.

A major feature of the Crocco-Lees solution is the appearance of a saddle-point singularity (the critical point) in the recompression region. This singularity is interpreted as being analogous to choking in the throat of a nozzle, i.e., the wake flow upstream of the singularity is subcritical and can transmit disturbances in the upstream direction. The wake flow downstream of the singularity is supercritical, i.e., supersonic on the average. The correct near-wake solution is taken as that which will pass through the singularity.

Although applicable to a broad class of strong viscous interaction problems, the original Crocco-Lees analysis yields rather poor results for planar turbulent near wakes. The first successful extension of the Crocco-Lees framework to the planar turbulent near-wake problem was made by Alber (Refs. 6 and 7). Alber obtained the integral parameters of the viscous flow profiles by using, in a transformed incompressible flow, the Stewartson solutions of the Falkner-Skan equations. The empirical mixing coefficient of the original Crocco-Lees analysis was replaced by the solution of the first moment of momentum equation (the mechanical energy equation); the dissipation integral in this equation was evaluated by the use of an empirical eddy viscosity model. Prandtl-Meyer coupling with the external flow was retained.

It is only recently that an attempt has been made to extend the Crocco-Lees framework to axisymmetric turbulent wake flows. Strahle and his coworkers (Refs. 8 and 9) have been developing an axisymmetric version of Alber's analysis, with the objective of extending it to the external burning populsion problem. The external flow is assumed to be isentropic and is treated with an approximate method of characteristics technique. (Prandtl-Meyer coupling is not applicable to axisymmetric flow). Only flows without base

bleed are considered. The solution for only one axisymmetric flow field has been presented (Ref. 9).

Korst model - The Korst component model (Ref. 5) is much simpler than the Crocco-Lees model and can be considered a first-order solution. The component processes involved in the near-wake flow field (inviscid external flow, turbulent mixing, recompression) are considered separately. The results from the component analyses are then combined to yield a solution for the base pressure and for the other global properties of the recirculating flow region. Three major assumptions are involved in the basic Korst analysis: (1) the recirculation region is quasi-stagnant, (2) the flow along the "discriminating" streamline (that which separates the flow which passes through recompression from that which is recirculated upstream) isentropically recompresses, and (3) the flow along the discriminating streamline stagnates at the peak of the recompression pressure distribution. Although experimental evidence is available to show that the first and third of these assumptions are quite incorrect, the basic Korst analysis (especially the simplest version in which initial boundary-layer effects are neglected) yields surprisingly good predictions of the base pressure for planar and quasi-planar flows. The analysis has been extended to include base bleed, asymmetrical two-stream flows, nonadiabatic flows, and flows with chemical reactions in the near wake (Ref. 10).

Numerous attempts have been made to improve the component analyses in the Korst model. Nash (Ref. 11) introduced an empirical factor to account for the fact that the discriminating streamline does not stagnate at the peak of the pressure distribution. Other investigators (e.g., Lamb and Hood, Ref. 12) have developed control volume analyses for the recompression region.

The basic assumptions in the basic Korst analysis are not very realistic. Because of compensating effects, the simplest Korst analysis for negligible initial boundary layers yields fairly satisfactory base pressure predictions for experimental flows with initial boundary layers of moderate thickness (δ less than the base height). Attempts to properly include the influence of the initial boundary layers in the Korst analysis, using techniques such as the apparent mixing layer origin shift concept of Hill and Page (Ref. 13), have not been very successful. However, these methods work reasonably well when applied to a mixing process which does not involve a large expansion at the base plane. The discrepancy for near-wake flows is related to the fact that the origin shift concept includes the change in the boundary-layer mean flow profile when it passes through the corner expansion process, but does not take into consideration that the boundary-layer turbulence decays rapidly when it passes through the expansion. This rapid decay of the turbulent fluctuations in the "remnant" of the initial boundary layer was observed experimentally by Lewis and Behrens (Ref. 14) and Page and Sernas (Ref. 15). These

observations lead to the conclusion that the boundary-layer flow after the corner expansion should not be taken as the initial condition for the subsequent development of the free turbulent mixing layer. Instead, the remnant of the boundary layer behaves as a rotational but inviscid external flow, and a new turbulent layer begins to develop at the edge of this rotational flow.

Several attempts have been made to apply the Korst method to the axisymmetric base pressure problem. If the method of characteristics is used to compute the inviscid flow adjacent to the constant pressure portion of the wake flow, then the solution cannot be extended to the axis. Therefore, several investigators (e.g., Ref. 16) have used the assumption that the flow recompresses, in a locally planar process, on an imaginary sting which extends from the base. Mueller (Ref. 17) assumed that recompression occurs either on a sting with a radius of one-half of the base radius, or on a sting equivalent in radius to the experimental radius of the wake after recompression; the latter radius was determined as an empirical function of the free-stream Mach number.

The simple recompression concepts of the original Korst theory are poorly suited for the computation of axisymmetric near-wake flows. However, there are enough free parameters in the axisymmetric extensions of the Korst model so that reasonably adequate values for the base pressure can be obtained. But these models really are used to correlate experimental base pressure measurements rather than to predict them. Moreover, the Korst-type models do not provide any information about the detailed flow structure in the recompression region.

Other methods - McDonald (Ref. 18) took a unique approach to the prediction of the planar base pressure for flows which reattach to a solid wall. (The centerline of Fig. 1 is replaced by a wall). McDonald also applied his analysis to axisymmetric flows in which a relatively large sting extends downstream from the base (Ref. 19). The base pressure is uniquely determined as that which causes the reattached flow downstream of recompression to become a fully developed flat plate boundary layer. Although McDonald produced reasonable predictions of the base pressure, his model can be criticized on physical grounds. Numerous experiments have shown that the planar near-wake structure for reattachment to a plane of symmetry is not significantly different from that for reattachment to a wall. Therefore, wall viscous effects cannot be a major controlling factor in the near-wake structure.

Chow (Ref. 20) has developed a two-layer integral treatment of recompression in planar flow; in many aspects, this physically realistic model combines features of both the Crocco-Lees and Korst models. Chow found it necessary to include the lateral pressure gradients in the recompressing viscous layer; however, this need to include lateral pressure gradients is probably related to the assumed geometry of the dividing streamline.

This recompression analysis is applicable only to the region upstream of the RSP (Fig. 1). The predictions of the Chow model are discussed in Section 3.0.

Recently, Chow and Spring (Ref. 21) developed a method for predicting the wake development downstream of the RSP. In addition, they improved the computation of the turbulent mixing upstream of the onset of recompression, and quite good predictions of planar base pressures were obtained.

Weng (Ref. 22) has extended the Chow recompression model to axisymmetric wake flows in which a sting extends from the base; it seems that this model should, in principle, also apply to flows without a sting. In common with the models of Chow and of Chow and Spring, the finite recirculation velocities are neglected in the flow upstream of the recompression region. The external flow is computed by the method of characteristics downstream to the onset of recompression; Prandtl-Meyer coupling is used in the recompression region. The initial boundary-layer profile after the base expansion process is taken as the initial condition for the development of the free shear layer. Weng used Prandtl mixing length theory to compute the turbulent shear stresses in the flow upstream of the onset of recompression; in the recompression region, he used an arbitrary spatial variation of the eddy viscosity.

Weng obtained reasonably good predictions of the effect of sting-base radius ratio on the base pressure for free-stream Mach numbers from 1.5 to 2.5.

Summary of Earlier Analytical Work - Of the available analytical models for planar wake flows, those of Alber (Refs. 6 and 7) and Chow and Spring (Ref. 21) are the most perceptive. Both models provide a prediction of the flow-field structure as well as of the base pressure. The Chow and Spring model provides the best prediction of the effect of initial boundary layer on the base pressure over the Mach number range investigated, but Alber's model is attractive because finite reverse flow velocities are included in the region upstream of the onset of recompression. Neither of these models has been applied to flows with base bleed; indeed, only the Korst-type models have been used to predict the effects of base bleed.

Of the available models for axisymmetric wake flows, only those of Strahle, et al. (Refs. 8 and 9) and Weng (Ref. 22) are based on a reasonably adequate description of the detailed flow processes. Strahle, et al., have not yet included initial boundary-layer effects in their model. As discussed in Section 3.0, Weng's method of computing the initial boundary-layer effect will probably be inadequate for free-stream Mach numbers of three or greater.

It is clear that even the recently developed models for axisymmetric flow do not satisfy the criteria established in Section 1.1 for a generalized near-wake analysis. The void between the requirements and the capabilities of available models was even more pronounced at the time that the work described in this report was initiated. Therefore, it was decided to undertake the development of an analytical model which would be applicable to a broad range of supersonic near-wake flows (Section 1.1).

1.3 IMPORTANT FEATURES OF A REALISTIC ANALYTICAL MODEL

When one considers the earlier analytical work, as well as the available experimental information, it becomes clear that a perceptive model of the near-wake structure should include several features. First, adequate treatment of the external flow in the axisymmetric case requires the use of the method of characteristics. Second, the evidence on quenching of the turbulence in the expanding boundary layer suggests that the remnant of the initial boundary layer can be computed with the rotational method of characteristics. Third, as shown by Weinbaum (Ref. 23), the viscous forces are negligible compared to inertial forces during the turning of the initial boundary layer, and the expansion of the supersonic portion of the initial boundary layer can be computed with the rotational method of characteristics. (A streamtube method can be used to compute the expansion of the subsonic portion of the initial boundary layer). Fourth, a new turbulent shear layer should be considered to begin after the corner expansion process. It should be noted that the concept of a new shear layer which develops downstream of the corner expansion has been suggested by Korst (Ref. 24) and has been used in the planar analysis of Chow and Spring (Ref. 21).

The available experimental evidence suggests that the near-wake region between the onset of recirculation and the beginning of recompression can be considered to be a constant pressure region, as has been assumed by most investigators. However, the experimental evidence does not suggest that the reverse flow velocities can be neglected, as has been done in the Korst-type models; the finite recirculation velocities must be included.

The analytical model which is described in Section 2.0 incorporates the features which have been discussed. The framework of the analysis is conceptually similar to the Crocco-Lees approach. However, the detailed treatment of the flow processes is closely related to the method used by the authors for ducted two-stream mixing flows (Refs. 25 and 26).

2.0 DEVELOPMENT OF ANALYTICAL MODEL

The geometry and nomenclature for the near-wake analysis is illustrated in Fig. 3. The flow downstream of the base is divided into three distinct regimes: (1) the "jet regime" which extends from the base plane to the station where recirculation begins, (2) the "wake regime" which extends from the onset of recirculation downstream to the onset of recompression, and (3) the "fully developed" regime which begins at the onset of recompression and extends downstream into the fully developed far-wake region.

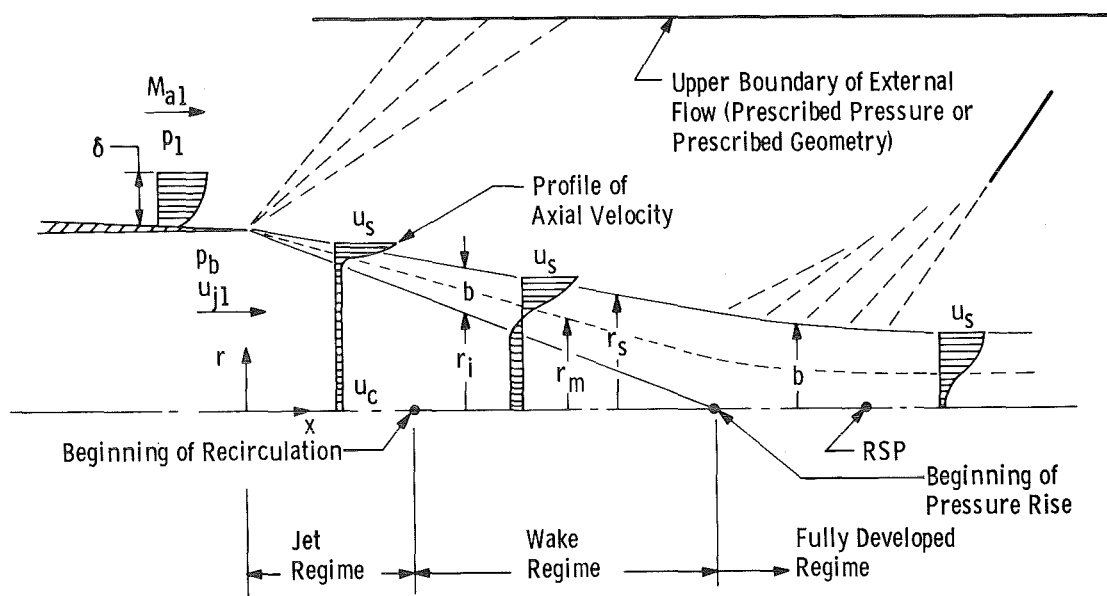


Figure 3. Nomenclature for near-wake analysis.

2.1 BASIC ASSUMPTIONS

The major assumptions used in the analysis are:

1. The flow is steady and is either planar or axisymmetric.
2. All gases obey the perfect gas law.
3. The integral form of the boundary-layer equations describes the flow between the axis and the outer edge of the turbulent mixing layer, r_s .
4. The turbulent Prandtl and Schmidt numbers are unity.

5. The free shear layer which forms downstream of the base expansion process is fully turbulent (negligible laminar transport) and has a negligible initial thickness.
6. The flow outside of the free turbulent shear layer ($r > r_s$) is supersonic, adiabatic, and inviscid.
7. The upper boundary of the supersonic external flow is inviscid and is either a prescribed geometry or has a prescribed constant pressure.
8. The normalized profiles of the axial component of velocity in the turbulent shear layer (between r_i and r_s) are similar and are represented by a cosine function.
9. The element species and axial component of velocity between the axis and r_i are one-dimensional.
10. The centerline static pressure in the jet regime is an isentropic function of u_c .
11. The centerline static pressure is constant in the wake regime.
12. The initial boundary layer is turbulent and is characterized by its thickness and a power law velocity profile.
13. Pressure feedback effects in the boundary layer upstream of the base are negligible.
14. The expansion of the initial boundary layer at the base plane is inviscid.
15. The base bleed flow is uniform and subsonic at the base plane.
16. Chemical reactions in the viscous wake flow, if they occur, are assumed to be in equilibrium.
17. If the planar flow reattaches to a wall rather than to a plane of symmetry, then viscous effects along the wall are negligible.

The use of the boundary-layer approximations (assumption 3) is consistent with Crocco-Lees and implies that (1) there are negligible lateral pressure gradients in the viscous wake flow, and (2) streamwise turbulent transport mechanisms are negligible. The assumption of negligible lateral pressure gradients is reasonably valid in the jet and wake regimes because the curvature of the streamlines is small in the high-speed portion of the

viscous layer; this assumption is less valid in the recompression region of the fully developed regime. The use of a cosine profile in the shear layer, along with a uniform reverse flow profile, was suggested by Green (Ref. 27) for incompressible wake flows. It should be noted that, even though the common term "base bleed" is used in this report, the momentum of the stream issuing from the base is not neglected; therefore, the analysis is applicable to "bleed" velocities in the high subsonic range.

2.2 BASIC EQUATIONS

The basic boundary-layer equations are:

Continuity

$$\frac{\partial}{\partial x} (\rho u r^a) + \frac{\partial}{\partial r} (\rho v r^a) = 0 \quad (1)$$

where

$a = 0$ for planar flow and

$a = 1$ for axisymmetric flow

Axial Momentum

$$\rho u r^a \frac{\partial u}{\partial x} + \rho v r^a \frac{\partial u}{\partial r} = \frac{\partial}{\partial r} (\tau r^a) - r^a \frac{\partial p}{\partial x} \quad (2)$$

where

τ is the turbulent shear stress

Element Species Conservation

$$\rho u r^a \frac{\partial C}{\partial x} + \rho v r^a \frac{\partial C}{\partial r} = \frac{\partial}{\partial r} (q r^a) \quad (3)$$

where q is a turbulent species flux.

Equations (1) through (3) are integrated (Ref. 25) to obtain five integral equations: (1) a continuity equation for the flow between the centerline and r_s , (2) a momentum equation for the flow between the centerline and r_s , (3) a momentum equation for the flow between the centerline and r_m (where $r_m = r_i + b/2$), (4) a species conservation equation for the flow between the centerline and r_s , and (5) a species conservation equation for the flow between the centerline and r_m . The integral equations are:

Overall Continuity

$$\int_0^{r_s} \frac{\partial}{\partial x} (\rho u) r^\alpha dr = - \rho_s v_s r_s^\alpha \quad (4)$$

Overall Momentum

$$\int_0^{r_s} \frac{\partial}{\partial x} (\rho u^2) r^\alpha dr = - \rho_s v_s u_s r_s^\alpha - \frac{dp_c}{dx} \frac{r_s^{\alpha+1}}{(\alpha+1)} \quad (5)$$

Half-Radius Momentum

$$\int_0^{r_m} \frac{\partial}{\partial x} (\rho u^2) r^\alpha dr - u_m \int_0^{r_m} \frac{\partial}{\partial x} (\rho u) r^\alpha dr = \tau_m r_m^\alpha - \frac{dp_c}{dx} \frac{r_m^{\alpha+1}}{(\alpha+1)} \quad (6)$$

Overall Species

$$\int_0^{r_s} \frac{\partial}{\partial x} (\rho u C) r^\alpha dr = 0 \quad (7)$$

Half-Radius Species

$$\int_0^{r_m} \frac{\partial}{\partial x} (\rho u C) r^\alpha dr - C_m \int_0^{r_m} \frac{\partial}{\partial x} (\rho u) r^\alpha dr = q_m r_m^\alpha \quad (8)$$

Because the flow is one-dimensional for $0 < r < r_i$, the integral equations can be rewritten as follows:

Overall Continuity

$$\int_{r_i}^{r_s} \frac{\partial}{\partial x} (\rho u) r^\alpha dr = - \rho_s v_s r_s^\alpha - \frac{r_i^{\alpha+1}}{(\alpha+1)} \frac{d}{dx} (\rho_c u_c) \quad (9)$$

Overall Momentum

$$\int_{r_i}^{r_s} \frac{\partial}{\partial x} (\rho u^2) r^\alpha dr = - \rho_s v_s u_s r_s^\alpha - \frac{dp_c}{dx} \frac{r_s^{\alpha+1}}{(\alpha+1)} - \frac{r_i^{\alpha+1}}{(\alpha+1)} \frac{d}{dx} (\rho_c u_c^2) \quad (10)$$

Half-Radius Momentum

$$\begin{aligned} \int_{r_i}^{r_m} \frac{\partial}{\partial x} (\rho u^2) r^\alpha dr - u_m \int_{r_i}^{r_m} \frac{\partial}{\partial x} (\rho u) r^\alpha dr &= \tau_m r_m^\alpha - \frac{dp_c}{dx} \frac{r_m^{\alpha+1}}{(\alpha+1)} \\ &- \frac{r_i^{\alpha+1}}{(\alpha+1)} \frac{d}{dx} (\rho_c u_c^2) + u_m \frac{r_i^{\alpha+1}}{(\alpha+1)} \frac{d}{dx} (\rho_c u_c) \end{aligned} \quad (11)$$

Overall Species

$$\int_{r_i}^{r_s} \frac{\partial}{\partial x} (\rho u C) r^\alpha dr = - \frac{r_i^{\alpha+1}}{(\alpha+1)} \frac{d}{dx} (\rho_c u_c C_c) \quad (12)$$

Half-Radius Species

$$\int_{r_i}^{r_m} \frac{\partial}{\partial x} (\rho u C) r^\alpha dr - C_m \int_{r_i}^{r_m} \frac{\partial}{\partial x} (\rho u) r^\alpha dr = q_m r_m^\alpha - \frac{r_i^{\alpha+1}}{(\alpha+1)} \frac{d}{dx} (\rho_c u_c C_c) + C_m \frac{r_i^{\alpha+1}}{(\alpha+1)} \frac{d}{dx} (\rho_c u_c) \quad (13)$$

Equations (9) through (13) apply to all three regimes of Fig. 3. Of course, r_i goes to zero in the fully developed regime, the pressure gradient terms are zero in the wake regime, and $C_c = C_j = 1$ in the jet regime.

2.3 SHEAR LAYER PROFILES

The free shear layer velocity profile is given by

$$\frac{u - u_c}{u_s - u_c} = \frac{1}{2} - \frac{1}{2} \cos \left(\pi \frac{r-r_i}{b} \right) \quad (14)$$

The velocity at the half-radius surface, $r_m (= r_i + b/2)$, is given by

$$u_m = u_c + \frac{1}{2} (u_s - u_c) \quad (15)$$

If the shear layer were at constant pressure, with constant values of u_s and u_c , then the element species concentration profile would be given by

$$C = A + B u$$

or

$$\frac{C - C_c}{C_s - C_c} = \frac{u - u_c}{u_s - u_c} \quad (16)$$

which is the well known Crocco integral solution obtained from Eqs. (2) and (3). In the near-wake problem, however, the pressure gradient terms are negligible only in the wake regime. In addition, C_c , u_c , and u_s vary with x , even in a region of constant pressure. Therefore, Eq. (16) cannot be used. The approach which has been taken in this study is to assume that the deviations from Eq. (16) can be expressed as

$$\frac{C - C_c}{C_s - C_c} = \left(\frac{u - u_c}{u_s - u_c} \right)^K \quad (17)$$

where K can vary with x . It should be noted that a power law relation similar to Eq. (17) has been used to compensate for the deviations from the Crocco relation which are

caused by nonunity transport coefficient ratios in free turbulent flows (Ref. 28). Since C_s is defined to be zero, Eq. (17) becomes

$$C = C_c - C_c \left(\frac{u - u_c}{u_s - u_c} \right)^K \quad (18)$$

2.4 COMPUTATION OF DENSITY IN THE VISCOUS FLOW

For unity turbulent Prandtl and Schmidt numbers, the stagnation enthalpy and the gas properties are uniquely related to C , and the density field is calculated with the techniques described in Ref. 25. The stagnation temperature, specific heat, and gas constant are specified as a function of C , which varies from zero (pure outer-stream gas) to one (pure base bleed gas). For chemically frozen flow, only the T_o , c_p and R values at $C = 0$ and at $C = 1$ need be specified. For flow with equilibrium chemical reactions, T_o , c_p and R are specified as functions of C .

At any point in the shear layer, u is given by Eq. (14), C is given by Eq. (18), and T_o , c_p , and R are then determined. The density can be obtained from the energy equation and the perfect gas law. Therefore, the density can be expressed functionally as

$$\rho = \rho(u, C, p) \quad (19)$$

2.5 TURBULENT TRANSPORT TERMS

The turbulent shear stress, τ_m , which appears in Eq. (11) is given by

$$\tau_m = \rho_m \epsilon \left. \frac{\partial u}{\partial r} \right|_m \quad (20)$$

where ϵ is the turbulent eddy viscosity. The eddy viscosity is given by

$$\epsilon = \frac{1}{R_T} b |u_s - u_c| \quad (21)$$

where R_T is a turbulent Reynolds number based on the eddy viscosity, the shear layer width and the velocity difference across the layer; the model used to obtain R_T is described in Section 2.12.

The equation for τ_m becomes, for the cosine velocity profile,

$$\tau_m = \frac{\pi}{2R_T} \rho_m |u_s - u_c| (u_s - u_c) \quad (22)$$

The turbulent species flux, q_m , is given by

$$q_m = \rho_m \epsilon \left. \frac{\partial C}{\partial r} \right|_m$$

or

$$q_m = - \frac{\pi}{2R_T} \rho_m |u_s - u_c| C_c K (0.5)^{K-1} \quad (23)$$

2.6 TRANSFORMATION OF THE INTEGRAL EQUATIONS

Jet regime - Assuming that the flow conditions along r_s can be specified, sufficient information is available to relate the terms in Eqs. (9) through (13) to four flow-field variables. Since there are only four unknowns in the jet regime, Eq. (13) is not used. The four dependent variables were selected to be p_c , r_i , b and K . Equations (9) through (12) can be transformed into the following system (Refs. 25 and 29)

$$N_1 \frac{dp_c}{dx} + N_2 \frac{dr_i}{dx} + N_3 \frac{db}{dx} + N_4 \frac{dK}{dx} = N_5 \quad (24)$$

where $N \equiv F$ for the continuity equation, $N \equiv G$ for the overall momentum equation, $N \equiv H$ for the half-radius momentum equation, and $N \equiv I$ for the overall species conservation equation. The equations for the coefficients are presented in Appendix A. The numerous auxiliary equations necessary for computation of the coefficients are developed in the same manner as described in Ref. 25.

Equations (24) are solved for the derivatives (dp_c/dx , dr_i/dx , db/dx , dK/dx) by use of a matrix factorization technique. The resulting equations for the derivatives are numerically integrated with a modified Euler technique (variable step size).

Wake regime - The five dependent variables selected in the wake regime are u_c , r_i , b , K and C_c . Equations (9) through (13) are transformed into the following system:

$$N_1 \frac{du_c}{dx} + N_2 \frac{dr_i}{dx} + N_3 \frac{db}{dx} + N_4 \frac{dK}{dx} + N_5 \frac{dC_c}{dx} = N_6 \quad (25)$$

where $N \equiv J$ for the half-radius species equation. The equations for the coefficients are presented in Appendix A.

Fully developed regime - The five dependent variables selected in the fully developed regime are p_c , u_c , b , K and C_c . Equations (9) through (13) are transformed into the following system:

$$N_1 \frac{dp_c}{dx} + N_2 \frac{du_c}{dx} + N_3 \frac{db}{dx} + N_4 \frac{dK}{dx} + N_5 \frac{dC_c}{dx} = N_6 \quad (26)$$

The equations for the coefficients are presented in Appendix A.

2.7 SOLUTION OF THE OUTER FLOW AND COUPLING WITH THE VISCOUS LAYER

The supersonic flow in the region $r > r_s$ is computed with the rotational method of characteristics. The "reference plane" technique, in which the supersonic flow parameters are established along planes normal to the axis, is used. The axial location of the reference planes coincides with the axial stations used in the numerical integration of the viscous layer equations.

Many terms which appear in the coefficients, N , of the viscous layer equations depend on the flow conditions (and their derivatives with respect to x) along r_s , the interface between the viscous region and the outer supersonic flow. Therefore, the solution of the two regions must be coupled. The technique used for coupling the two regions is illustrated in Fig. 4. At some station, x , the flow in both regions is fully specified. In the integration technique for the viscous layer equations, the step size, Δx , is given, as are the tentative values of p and r_s at $(x + \Delta x)$. A left running characteristic, along which the flow is fully defined, is constructed from the the last boundary point (Fig. 4). The right running characteristic and the streamline, each of which passes through the new boundary point and intersects the left running characteristic, are constructed; the equations for the streamline and the right running characteristic are solved in the usual iterative manner to define the entropy and flow angle at the new boundary point. Then the density and velocity at the new boundary point are computed, and the derivatives with respect to x of these flow properties along r_s are computed with an upstream differencing technique. (These derivatives are assumed to be zero at $x = 0$). Therefore, sufficient information is available about the flow properties along r_s so that the coefficients of the viscous layer equations at $(x + \Delta x)$ can be evaluated.

Within the framework of the Euler integration technique, this boundary point procedure is repeated, with different values of p_c and r_s at $(x + \Delta x)$, until the solution of the viscous equations converges. The solution then proceeds downstream to a new axial station. In this downstream marching procedure, development of the solutions for the two flow regions is fully coupled.

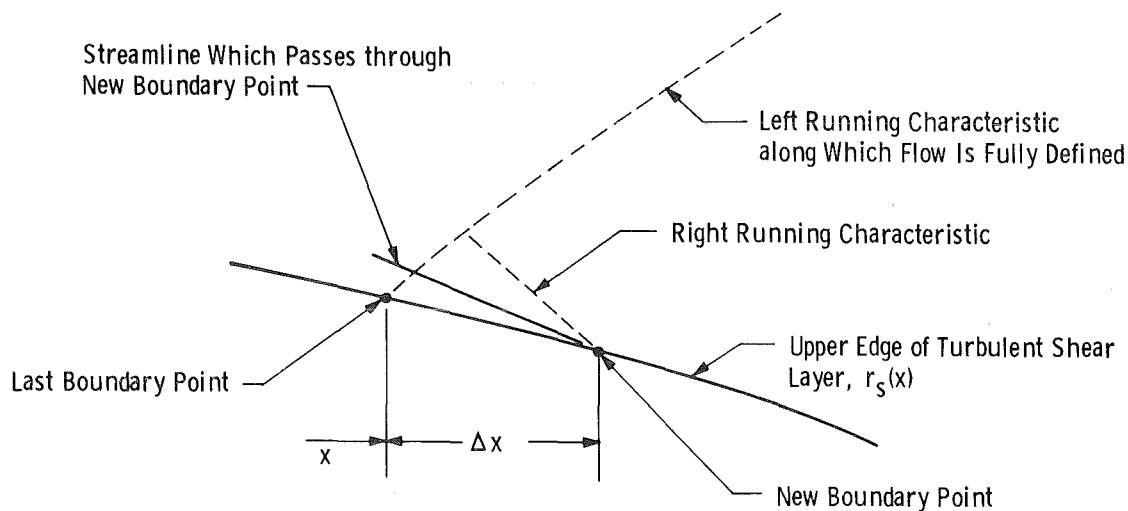


Figure 4. Coupling of the shear layer and outer-flow solutions.

Even though the outer flow is treated with the rotational method of characteristics, no shock waves are allowed to develop. However, two shock waves exist even in simple near-wake flow fields, the lip shock and the recompression shock. The lip shock, which has been experimentally investigated by Hama (Ref. 30), results from the overturning of the low Mach number portion of the initial boundary layer in the base expansion process (Ref. 23). In neglecting the lip shock, we have treated it as an isentropic compression which is justified since experiments have shown that the lip shock is rather weak, at least for free-stream Mach numbers up to 2.0 or 3.0.

The series of compression waves which result from the recompression process coalesce to form the recompression shock wave (Fig. 1). However, the shock is formed too far downstream to affect the near-wake closure mechanism. Therefore, neglecting the recompression shock wave influences only the downstream portion of the recompression process.

Inclusion of the lip and recompression shock waves in the present analysis is quite feasible, but would require a significant increase in the computation time.

2.8 EXPANSION OF THE INITIAL BOUNDARY LAYER

The expansion of the supersonic portion of the initial boundary layer (Fig. 5) is computed with the rotational method of characteristics. Since pressure feedback effects are neglected, the supersonic expansion process is initiated at $x = 0$ with a Prandtl-Meyer

turn (from p_1 to p_b) at the sonic point in the boundary layer. Expansion of the subsonic portion of the initial boundary layer is computed with an isentropic streamtube model. The subsonic layer is divided into ten streamtubes, each of which expands isentropically from p_1 to p_b . The flow direction of the streamtubes after expansion is taken to be the same as that of the initially sonic streamline after it passes through the Prandtl-Meyer turn. The flow in the wall streamtube, after expansion, is the initial edge condition (at $x = 0$) for the new turbulent shear layer which develops downstream of the base.

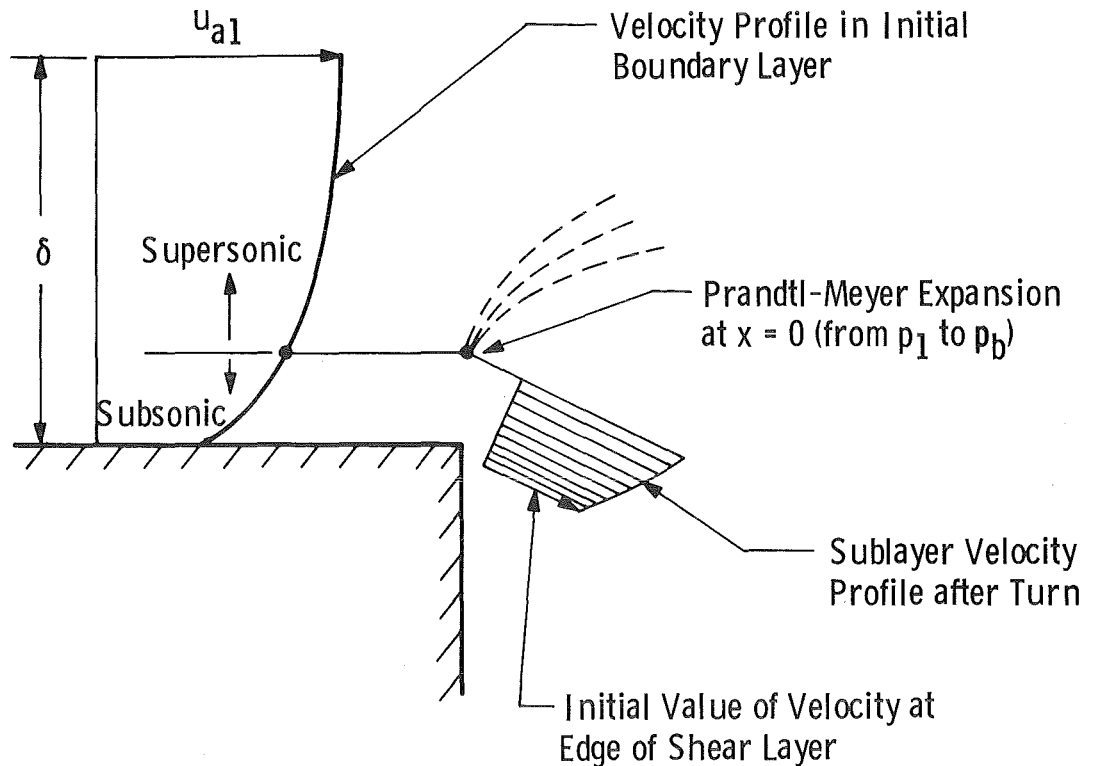


Figure 5. Corner expansion of the initial boundary layer.

For values of p_b/p_1 greater than the sonic static-total-pressure ratio, one or more of the streamtubes will be subsonic after the expansion process. In such cases, the Mach number of the subsonic streamtubes is arbitrarily adjusted to be slightly greater than unity. The effect of this adjustment process is very small for typical initial boundary-layer thicknesses because the mass flow in the adjusted streamtubes is small and is quickly entrained by the turbulent shear layer.

2.9 CHARACTERIZATION OF THE INITIAL AND BOUNDARY CONDITIONS

The turbulent near-wake flow field is fully determined by the following conditions, which must be specified:

1. The upper boundary of the supersonic external flow,
2. The base bleed flow rate,
3. The total temperatures and gas properties of the external flow and the bleed flow,
4. Mixture gas properties and total temperature as a function of C , if chemical reactions occur (Section 2.4),
5. Thickness, δ , and velocity profile shape of the adiabatic initial boundary layer, and
6. The profiles at the base plane of the static pressure, total pressure and flow angle, between the edge of the boundary layer and the upper boundary.

For computation of near-wake flows embedded in external flows of large lateral extent (effectively infinite), the upper boundary is specified as a wall parallel to the centerline and located far enough from the near wake so that reflected waves from the corner expansion process do not interact with the recompression region.

The initial boundary-layer velocity profile is assumed to be given by a power law

$$u/u_{a1} = (y/\delta)^n$$

where u_{a1} is the velocity at the edge of the boundary layer, δ is the thickness of the layer, y is the distance from the wall (Fig. 3), and n is specified.

The initial boundary-layer characteristics for near-wake experiments are usually specified in terms of the momentum thickness and the momentum thickness Reynolds number, Re_θ . Therefore, a method was developed to estimate n as a function of M_{a1} and Re_θ . Maise and McDonald (Ref. 31) showed that supersonic boundary-layer profiles on an adiabatic flat plate can be well represented by the Coles law-of-the-wall/law-of-the-wake profiles, along with the Van Driest transformed velocities and the Spalding-Chi skin friction values. The θ/δ values shown by Maise and McDonald as a function of M_{a1} and Re_θ , were matched with θ/δ values for power law profiles (Ref. 32) to determine n as a function of M_{a1} and Re_θ (Fig. 6). The relation of n , M_{a1} , and θ/δ is shown in Fig. 7.

The power law profile, as well as the profile used by Maise and McDonald, does not smoothly join the external stream velocity profile. The resulting "corner" on the total-pressure profile was found to cause computational problems in the viscous layer solution when the corner is entrained into the shear layer. To alleviate this problem, the outer edge of the initial boundary-layer velocity profile is smoothed with a cubic function which extends from $(r_b + 0.8\delta)$ to $(r_b + 1.2\delta)$. This smoothing has a negligible effect on the momentum thickness.

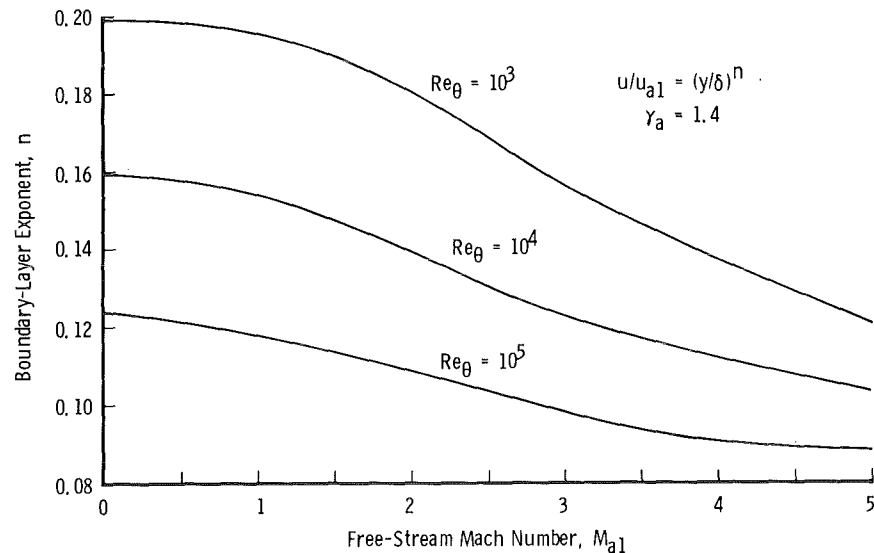


Figure 6. Boundary-layer profile exponent for adiabatic flow along a flat plate.

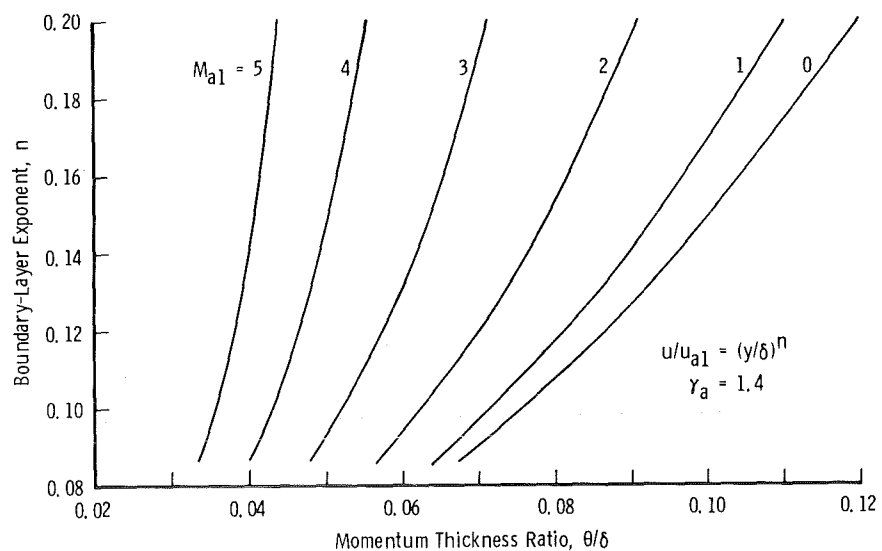


Figure 7. Boundary-layer momentum thickness ratio for adiabatic flow along a flat plate.

2.10 TWO-LAYER TREATMENT OF THE OUTER FLOW

It was discovered early in this investigation that the entropy profile in the initial boundary layer tends to spread into the outer flow, which is usually irrotational. Of course, the diffusion of the entropy field across streamlines is incorrect since the flow is assumed to be inviscid. Apparently, this false diffusion in the method of characteristics flow field is related to the rapid expansion of the highly rotational boundary-layer flow. The false diffusion effect is not unique to the present method of characteristics formulation; other widely used method of characteristics computer programs were found to yield similar results.

To eliminate the spurious entropy diffusion, a two-layer technique is used (Fig. 8). The streamline which originates at the outer edge of the initial boundary layer is established, and the total pressure on this streamline is specified to be p_{0a} . Therefore, the entropy field in the supersonic flow is divided into two layers, and the entropy gradients from the initial boundary layer are confined to the lower layer.

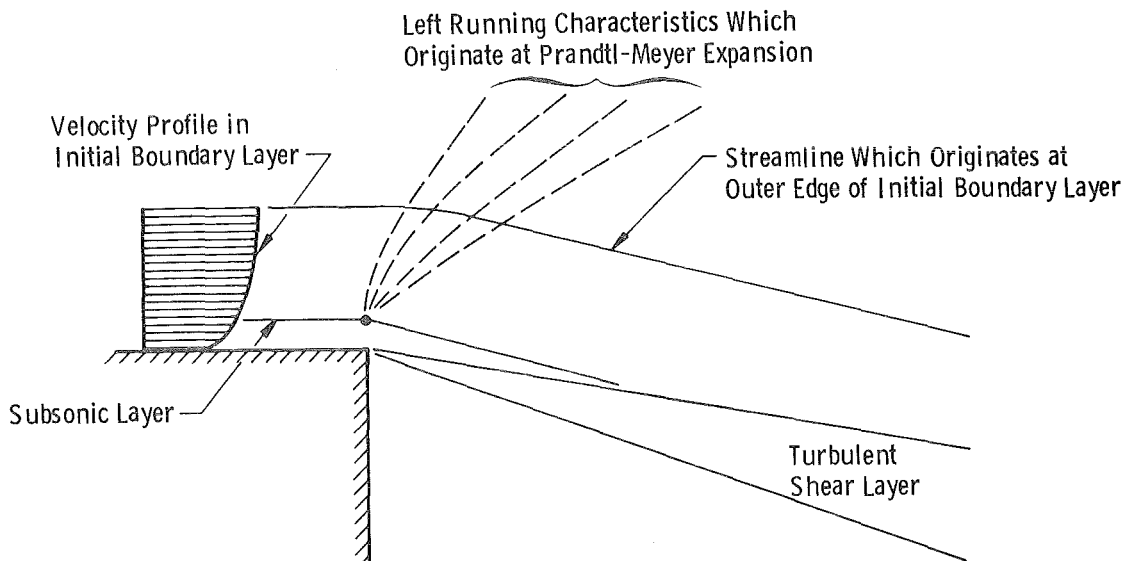


Figure 8. Two-layer treatment of the supersonic flow field.

2.11 METHOD OF SOLUTION

As in the Crocco-Lees analysis, a saddle-point singularity (the critical point), which is intrinsic to the solution, occurs in the reattachment region. The behavior of the solution is illustrated by the axial distribution of centerline velocity (Fig. 9). The correct solution is that which passes smoothly through the singularity. If the assumed base

pressure is too low the solution will be supercritical and "blow up", i.e., in terms of Cramer's rule, the determinant of the coefficients for Eqs. (26) will go to zero before the numerator determinants do. If the assumed base pressure is too high, the solution will be subcritical and is characterized by the centerline velocity reaching a maximum, then decreasing with distance (Fig. 9). By iterating on the initial conditions (base pressure), one can converge on the set of initial conditions which will cause the flow-field solution to pass smoothly through the singularity.

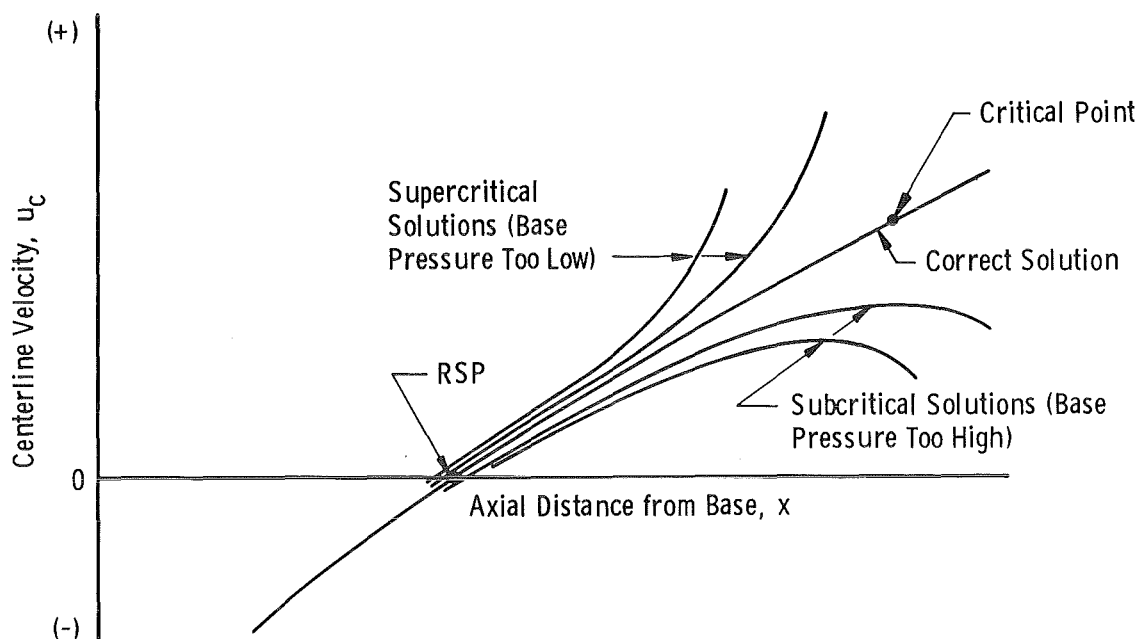


Figure 9. Subcritical and supercritical solutions.

The subcritical solutions are identified by du_c/dx going to zero. The supercritical solutions are identified by an inflection in the centerline velocity distribution, i.e., by d^2u_c/dx^2 going to zero, which implies that the determinant is approaching zero. A halving technique, with the bounds established by the last subcritical and the last supercritical values of p_b , is used to converge to the correct value of p_b . With a reasonable first guess on the bounds for p_b , say within 20 percent of the correct value, the converged value of p_b can be identified to within 0.5 percent with approximately ten iterations of the flow-field solution.

Although it is not difficult to define the initial conditions with practical engineering accuracy, establishing the solution through and beyond the critical region is very difficult. The nature of a saddle-point singularity is such that very small changes in the initial conditions result in large changes in the solution as the singularity is approached. Two

techniques have been used to obtain solutions which pass through the critical region. The first is a "brute force" approach; the correct initial condition is established with a very small tolerance, typically to within one part in 10^5 . At a station just upstream of the critical region, the centerline velocity is perturbed upward by a small amount (typically one percent) and the solution will usually proceed smoothly through the critical region. This procedure has been found to work fairly well for planar flows, and for axisymmetric flows with high external stream Mach numbers. However, for axisymmetric flows with moderate external stream Mach numbers (2.0 or 3.0), this procedure has not been successful, even when the initial conditions are converged to within one part in 10^6 .

An alternate approach for developing the solution through the critical region is to converge the initial conditions fairly tightly, perhaps to within one part in 10^3 or 10^4 , then to extrapolate the centerline velocity distribution. Results at two axial stations near the RSP, which is well upstream of the critical point, are used to establish an exponential extrapolation equation for $u_c(x)$. One equation, the continuity equation, is removed from Eqs. (26), and the singular behavior of the solution is removed. Experience has shown that the exponential extrapolation can be extended downstream, with good results, to the peak of the centerline pressure distribution in axisymmetric flow.

Results obtained with both of the techniques for developing the solution through the critical region are presented in Section 3.0.

Fortunately, the engineer is usually interested only in a prediction of the initial conditions (the base pressure). The initial conditions, and the flow field downstream to the vicinity of the RSP, can be determined with reasonable accuracy without developing the solution through the critical region.

The occurrence of the saddle-point singularity in the solution is a result of the elliptic nature of the near-wake flow field. That is, an essentially elliptic problem is treated as an iterative initial value problem, and the critical point is the mechanism whereby the downstream wake closure conditions are manifested.

The near-wake analysis has been programmed for numerical solution with an IBM 370-165 computer. A typical computation, for one assumed set of initial conditions, which proceeds from the base plane to downstream of the RSP requires a computation time of from 30 to 60 seconds. The determination of the base pressure to practical engineering accuracy (less than one percent uncertainty) involves a computation time of five to ten minutes.

For near-wake flows in which there is no base bleed, or in which the base bleed gas has the same total temperature and gas properties as the outer flow, a simplified version

of the computer program is used. The concentration equations are not solved, and K and C_c are set at unity. This simplified analysis is referred to as the "single gas" version.

2.12 MODEL FOR THE TURBULENT REYNOLDS NUMBER

As with any turbulent flow problem, the near-wake analysis requires an adequate model for the turbulent transport properties. Early in this investigation, an attempt was made to incorporate an integral formulation of the turbulent kinetic energy (TKE) equation into the near-wake analysis. This TKE formulation has been shown to yield very good results for a variety of constant pressure-free turbulent flows (Ref. 33). But the results for supersonic near-wake flows were very poor; the turbulent shear stress levels in the reattachment region were grossly underpredicted. The failure of the TKE formulation is attributed to the "extra strain" effects described by Bradshaw (Ref. 34). He points out that additional strains in the flow, in addition to the basic $\partial u/\partial r$ strain, have a disproportionately large effect on the turbulence structure. In the recompression region, the strains which result from both streamline curvature and dilatation (bulk compression) effects are significant.

Because of the failure of the TKE approach, we decided to develop an eddy viscosity model for the near-wake analysis, even though the history of eddy viscosity models (Ref. 35) indicates that such a model would probably have a limited range of applicability.

The eddy viscosity model described in Section 2.5 is the Prandtl model with the coefficient expressed as the inverse of the turbulent Reynolds number, R_T . In the jet and wake regimes, R_T is assumed to be a function only of the local Mach number, M_s , at the supersonic edge of the shear layer. The predictions of the integral TKE method (Ref. 33) agree well with the available experiments on the growth of planar shear layers with zero secondary velocity; the corresponding R_T values from the TKE analysis (Fig. 10) are well described by the function

$$R_T = 390 - 333 \exp(-0.495 M_s) \quad (27)$$

which is used in the jet and wake regimes.

The R_T model used in the fully developed regime is based on the experimental results of Mueller (Ref. 36) and Tani (Ref. 37) for incompressible reattaching planar flows. Their experimental configurations are shown in Fig. 11. The experimental velocity profiles were approximately fitted with a cosine function to estimate the width of the shear layer and the effective wall slip velocity. The results, along with the measured shear stress at the center of the velocity profile, were used to compute R_T . Two characteristic R_T values are of interest, the value at the beginning of reattachment, R_{Tp} and the value

at the RSP, R_{Tr} . (The beginning of reattachment is defined as the axial station where the wall static pressure is equal to the base pressure.) The values for R_{Tp} and R_{Tr} are shown below.

Experiment	R_{Tp}	R_{Tr}
Mueller, $h = 0.75$ in.	276	119
Mueller, $h = 0.50$ in.	216	106
Mueller, $h = 0.25$ in.	219	101
Tani, $h = 2$ cm	295	108

Because of the consistent values for R_{Tr} , from 100 to 120, we speculated that R_{Tr} would be a good parameter to characterize the level of the eddy viscosity in the reattachment region.

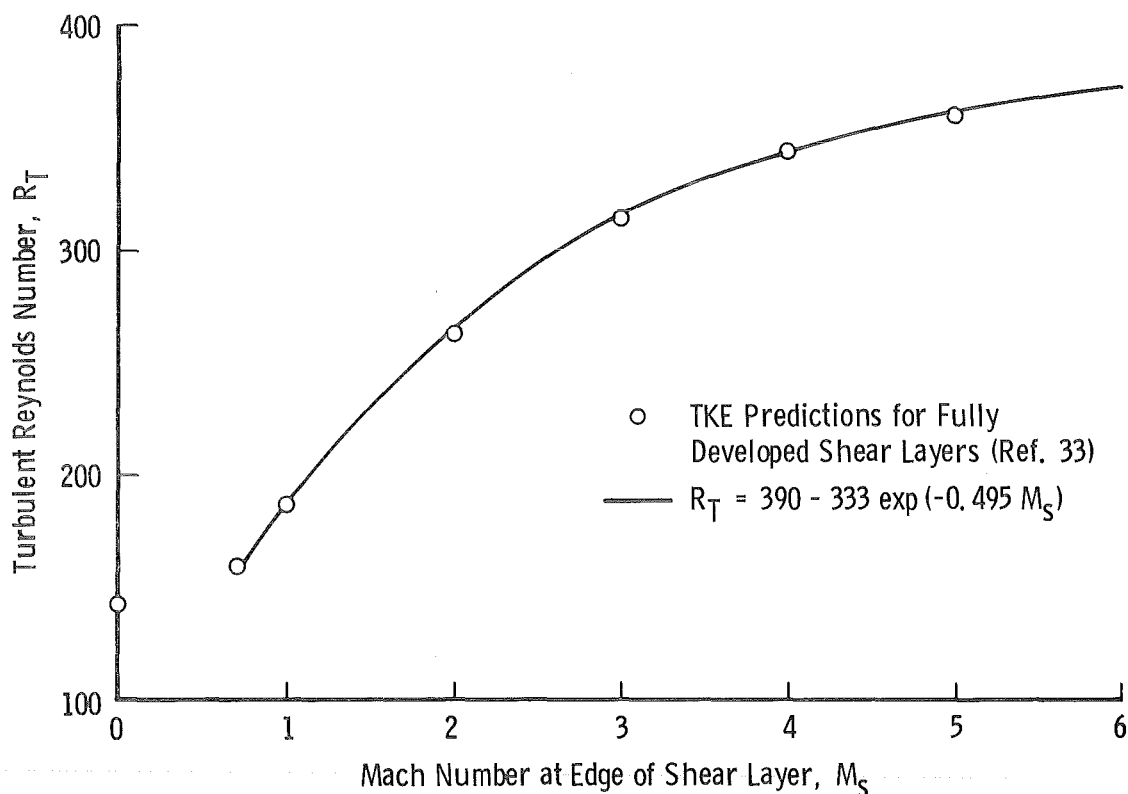
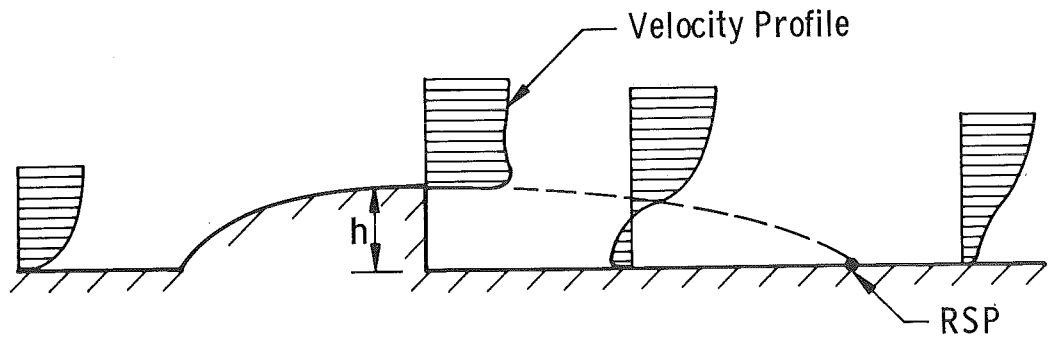
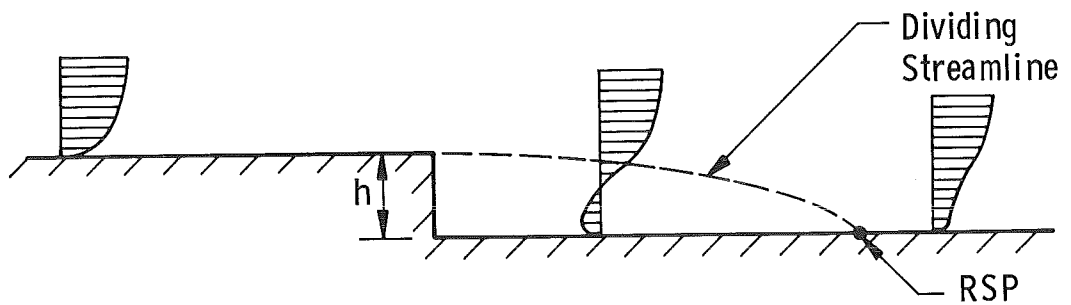


Figure 10. Turbulent Reynolds number for planar shear layers with no secondary flow.



a. Mueller's configuration



b. Tani's configuration

Figure 11. Configurations for low-speed separating and reattaching flow experiments.

From the experimental results of Mueller and of Tani, it was found that the distribution of R_T in the reattachment region could be taken to be a unique function of u_c/u_s ; u_s is the local velocity at the edge of the viscous layer and u_c is the effective wall slip velocity. Results are shown in Fig. 12 for the region between the beginning of reattachment and the RSP. The data are well represented by

$$(R_T - R_{Tr})/(R_{Tp} - R_{Tr}) = 0.6 \bar{u} + 0.4 \bar{u}^4 \quad (28)$$

where $\bar{u} = (u_c/u_s)/(u_c/u_s)_p$. Downstream of the RSP, the data (Fig. 13) are well represented by

$$R_T/R_{Tr} = \exp(-2.5 u_c/u_s) \quad (29)$$

In the near-wake analysis, Eqs. (28) and (29) are used to express the axial variation of R_T , and R_{Tp} is given by Eq. (27). Therefore, the level of the eddy viscosity throughout the fully developed regime is scaled by R_{Tr} .

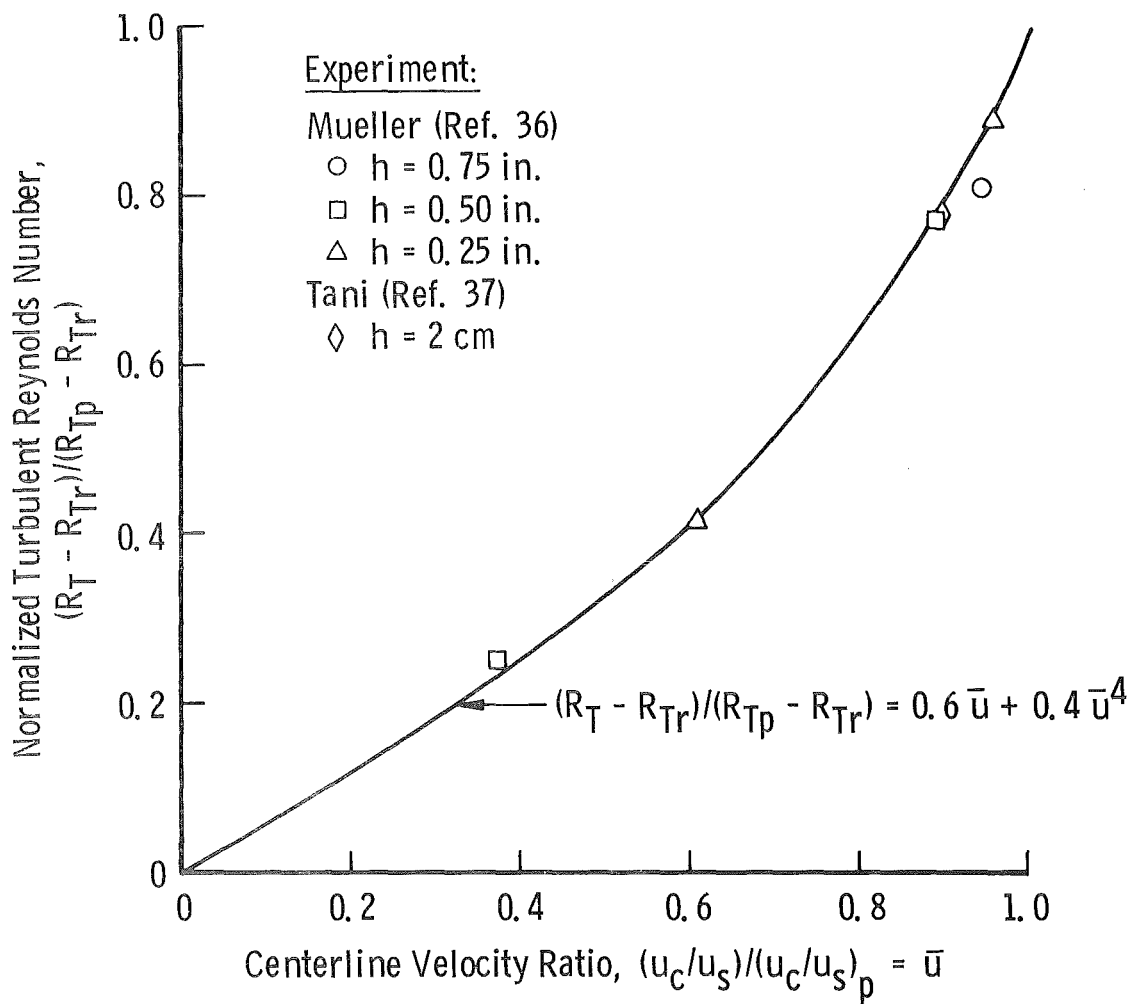


Figure 12. Turbulent Reynolds number distribution upstream of the RSP in the reattachment regime.

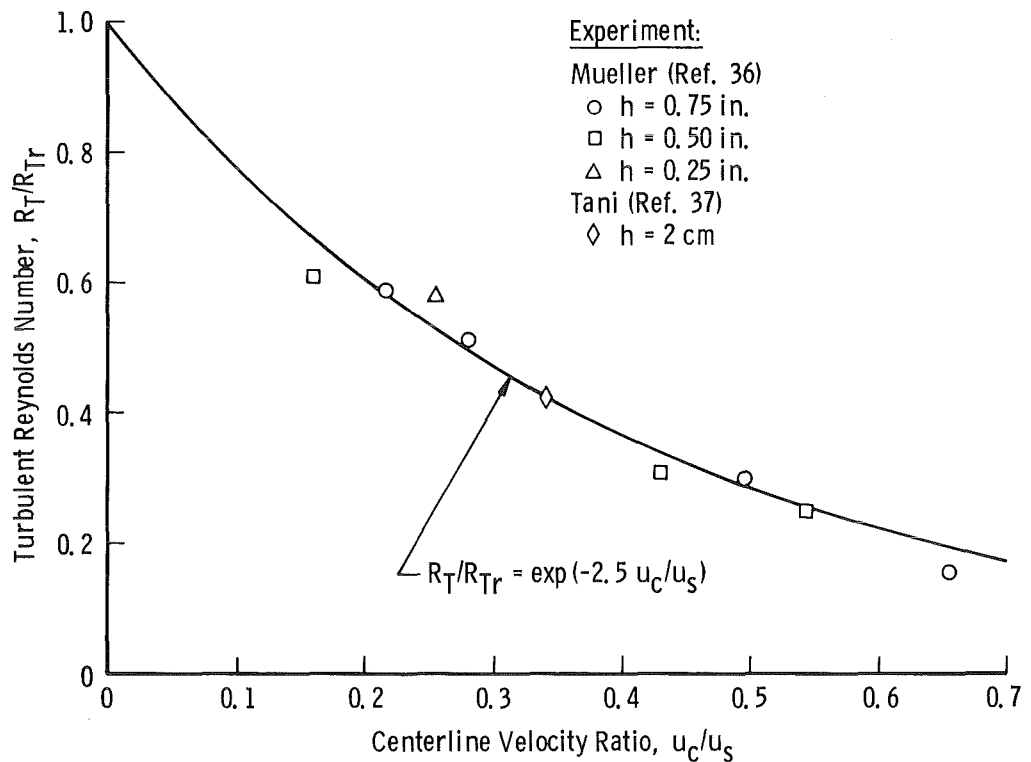


Figure 13. Turbulent Reynolds number downstream of the RSP.

A series of computational experiments was carried out to establish the values of R_{Tr} required to give a reasonably accurate prediction of experimental base pressures in supersonic flow (say to within five percent). The following matrix of test cases was selected:

Planar, $M_{a1} = 2.0$, $\theta/h = 0.016$

Planar, $M_{a1} = 2.0$, $\theta/h = 0.062$

Planar, $M_{a1} = 3.0$, $\theta/h = 0.013$

Axisymmetric, $M_{a1} = 2.0$, $\theta/h = 0.024$

Axisymmetric, $M_{a1} = 2.0$, $\theta/h = 0.053$

Axisymmetric, $M_{a1} = 4.0$, $\theta/h = 0.011$

Typical effects of R_{Tr} on the base pressure, for planar flow at $M_{a1} = 2$, are shown in Fig. 14. As would be expected, an increase in R_{Tr} (a decrease in the turbulent shear stress level) causes an increase in the base pressure.

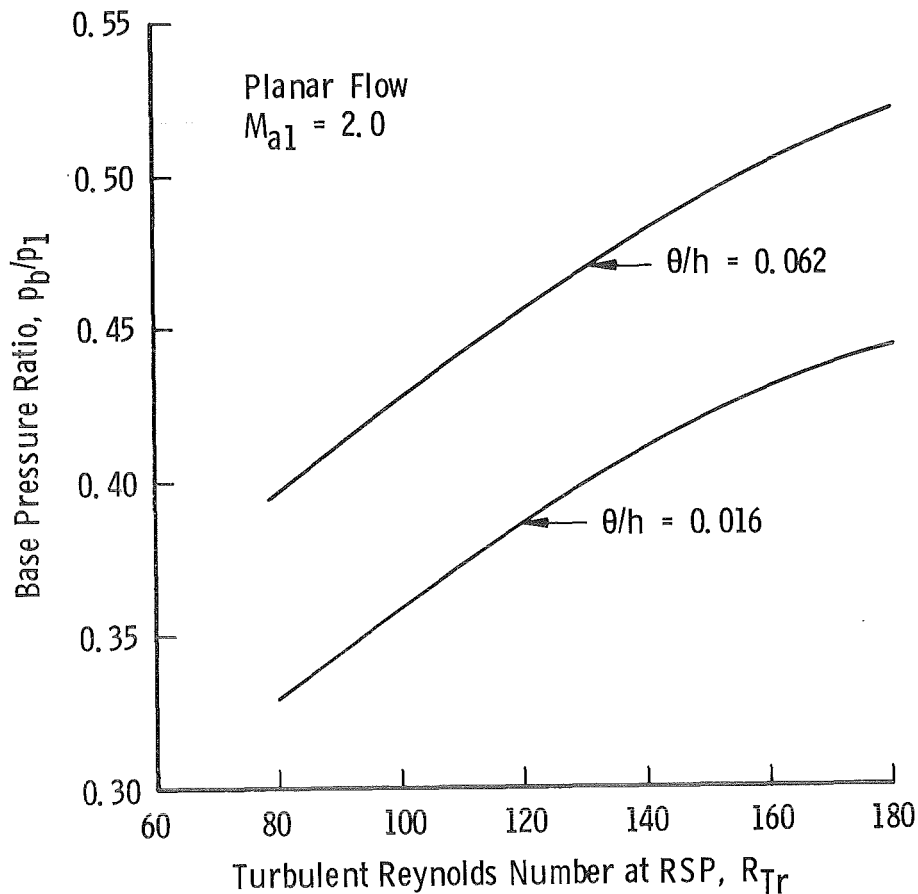


Figure 14. Influence of the turbulent Reynolds number at the RSP on the predicted base pressure.

From the matrix of base pressure test cases, it was found that R_{Tr} must decrease as the initial boundary-layer thickness is increased and as M_{a1} is increased. In addition, it was found that accurate prediction of axisymmetric flows requires a larger value of R_{Tr} than is required for planar flows. Since Bradshaw's curvature and dilatation strains are both related to a pressure gradient parameter, we decided to correlate R_{Tr} with a parameter proportional to the pressure gradient at the beginning of recompression. After some trial and error, the pressure gradient parameter was selected to be

$$\bar{P} = 2^{1-\alpha} \sqrt{M_{sp}} \delta_p dp_c/dx)_p / P_{cp} \quad (30)$$

where δ_p is the distance between the axis and the streamline which originates at the edge of the initial boundary layer. The results of the correlation of R_{Tr} with \bar{P} are shown in Fig. 15. Both curves which have been fitted to the required R_{Tr} values can be expressed by the following single equation:

$$R_{Tr} = 60 + 15\alpha + (40 + 135\alpha) \exp(-0.024 \bar{P}^{2.3}) \quad (31)$$

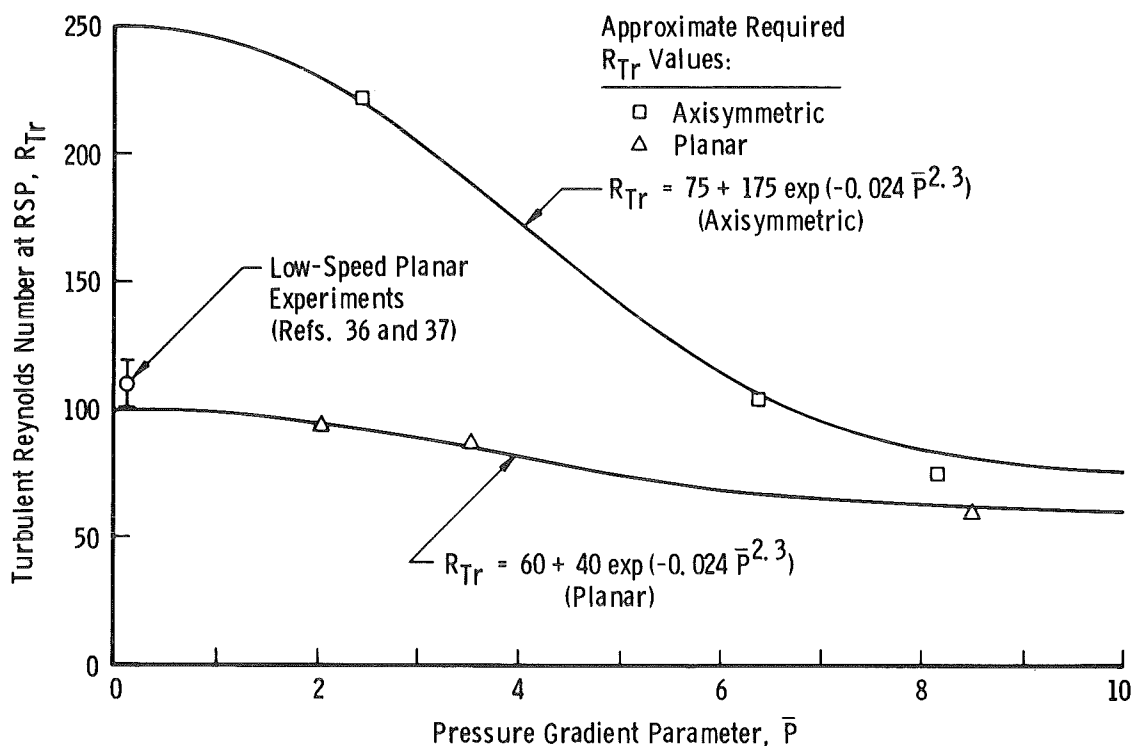


Figure 15. Turbulent Reynolds number at the RSP as a function of the pressure gradient parameter.

It is interesting that the required R_{Tr} values for planar flows (Fig. 15) at low values of \bar{P} are consistent with the low-speed experimental results of Mueller and of Tani.

It will be shown in Section 3.0 that the R_T model developed in this section yields good results for planar near-wake flows; in addition to the base pressure, the flow structure is predicted with adequate accuracy. However, the R_T model has been found to yield only fair results for axisymmetric flows with M_{a1} less than about 1.7; the predictions are fairly adequate at higher Mach numbers.

3.0 DISCUSSION OF RESULTS

In this section, the predictions of the near-wake model are compared with experimental results for planar and axisymmetric flows of the type shown in Fig. 2a; i.e., the supersonic external flow upstream of the base and outside of the wall boundary layer is uniform and parallel to the axis and is effectively infinite in lateral extent.

3.1 CONCENTRATION FIELD SOLUTION PROBLEMS

When attempts were made to compute near-wake flows for which the concentration equations must be solved, a singularity in the wake regime solution was encountered. Downstream of the onset of recirculation, the predicted centerline concentration, C_c , decays with axial distance. At some axial station upstream of the onset of recompression, the system of equations becomes singular; i.e., the determinant of the system of equations [Eq. (25)] goes to zero and the solution "blows up". This singularity is not related to the Crocco-Lees saddle-point singularity which occurs in the recompression region. Indeed, the new singularity does not exhibit saddle-point behavior; the solutions for all of the derivatives (dC_c/dx , etc.) remain smooth and monotonic as the singularity is approached.

The wake regime singularity does not appear to have physical significance, but is probably related to the particular formulation of the half-radius species equation or of the concentration profile shape function. The singularity also occurs when the concentration equations are solved for a single gas base bleed problem, even though no wake regime singularity occurs when the single gas version of the analysis is used for the same problem.

Strahle and Mehta (Ref. 8) encountered an extraneous singularity in their analysis of near-wake flows without base bleed. They were able to remove the singular behavior by changing their velocity profile functions in the region upstream of recompression (Ref. 9). Various modifications of the concentration profile function in the present analysis have been tried, but to no avail; the wake regime singularity occurs for both single gas flows and for flows in which the base bleed gas is different from the outer-stream gas. An obvious next step in attempting to solve this concentration field solution problem is to alter the formulation of the half-radius species equation.

Because of the unresolved problems in solving the concentration equations, only results from the single gas version of the near-wake model are presented in this report.

3.2 PLANAR BASE PRESSURE

The effect of initial boundary-layer momentum thickness on base pressure in planar flow is shown in Fig. 16 for $Ma_1 = 1.5$ and in Fig. 17 for $Ma_1 = 2.0$. The scatter shown in the experimental results is typical for planar flows and is attributed to sidewall effects which vary from experiment to experiment. At both free-stream Mach numbers, the present analysis predicts the experimental base pressures very well for θ/h less than 0.03 or 0.04. However, the analysis overpredicts the base pressure for higher values of θ/h ; the predicted values of p_b/p_1 are about ten percent too high at $\theta/h = 0.1$. In agreement with

experimental observations (Ref. 38) at free-stream Mach numbers of 1.5 and 2.0, the near-wake model predicts a negligible influence of Re_θ on the base pressure for a given value of θ/h . (Computations were made for Re_θ from 10^3 to 10^5).

The trend of p_b/p_1 versus θ/h predicted by the present analysis is similar to that predicted by Alber (Figs. 16 and 17); however, the present analysis provides significantly better predictions of the level of base pressure. The Chow theory (Ref. 20) predicts an incorrect trend of p_b/p_1 versus θ/h ; however, the Chow and Spring extension of this theory provides very good predictions of the base pressure at Mach numbers of 1.5 and 2.0 (Figs. 16 and 17).

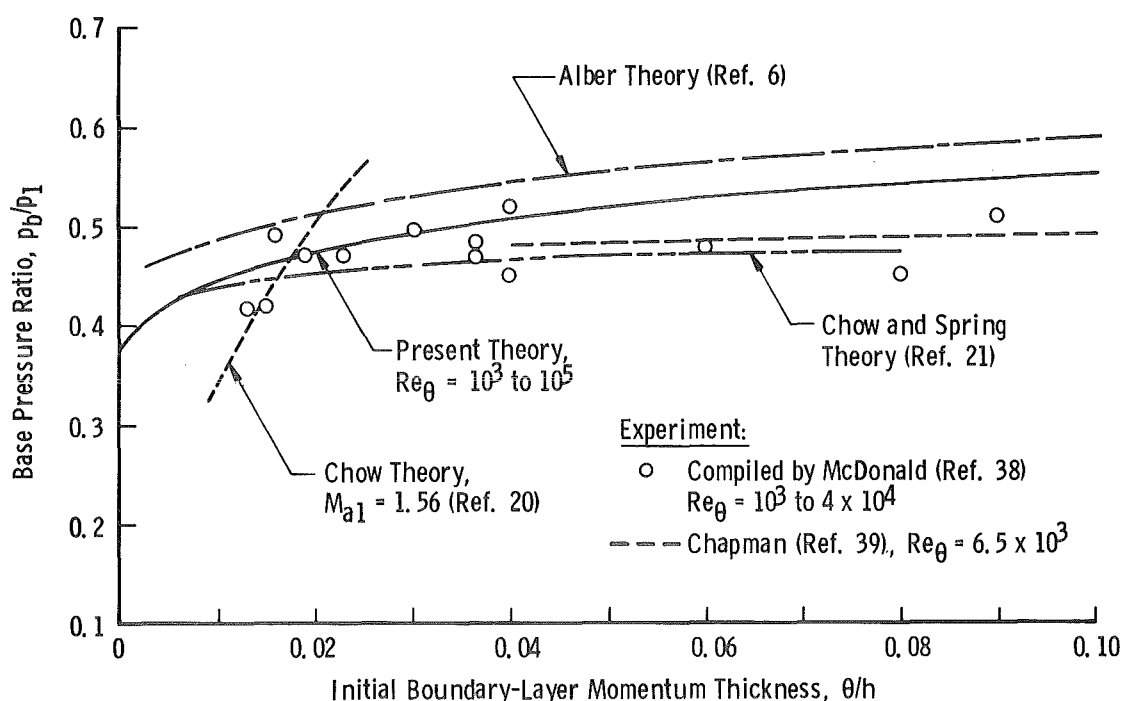


Figure 16. Effect of the initial boundary layer on the base pressure in planar flow ($M_{a1} = 1.5$).

Experimental base pressure results for $M_{a1} = 3.0$ (Fig. 18) show much more scatter than was observed at the lower Mach numbers. In agreement with the trend of the experimental results, the present analysis predicts a much larger effect of θ/h on the base pressure at $M_{a1} = 3.0$ than at $M_{a1} = 2.0$. In addition, a significant effect of Re_θ on the base pressure is predicted.

The effect of free-stream Mach number on the base pressure is shown in Fig. 19a for $\theta/h = 0.02$ and in Fig. 19b for $\theta/h = 0.04$. In view of the scatter in planar base pressure data, the predictions shown in Fig. 19 are very satisfactory.

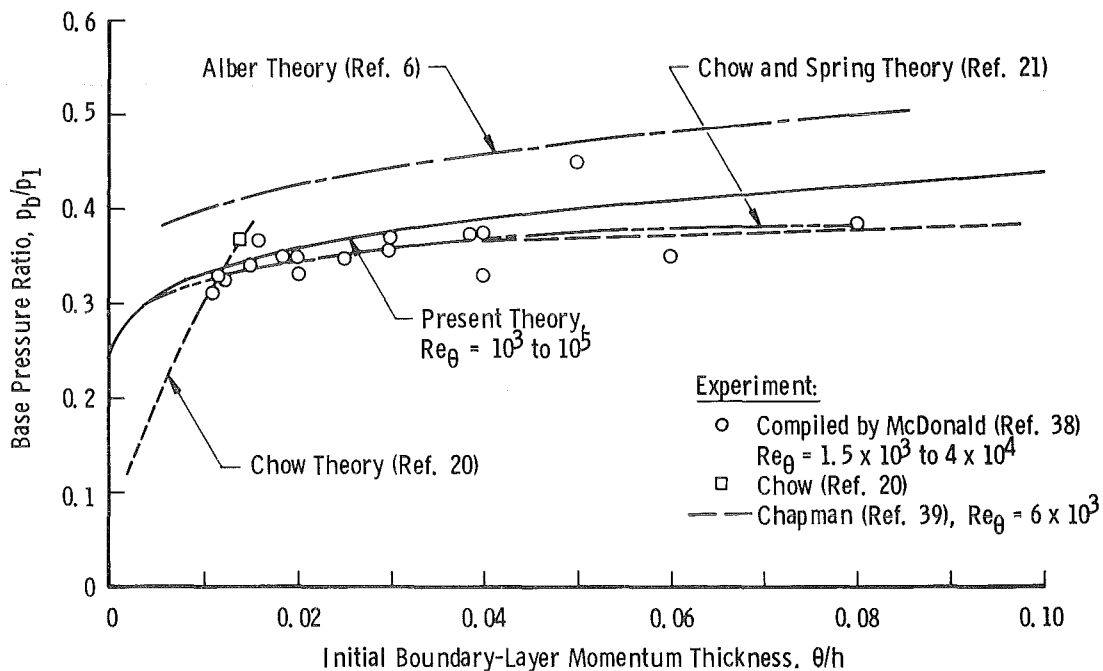


Figure 17. Effect of the initial boundary layer on the base pressure in planar flow ($M_{a1} = 2.0$).

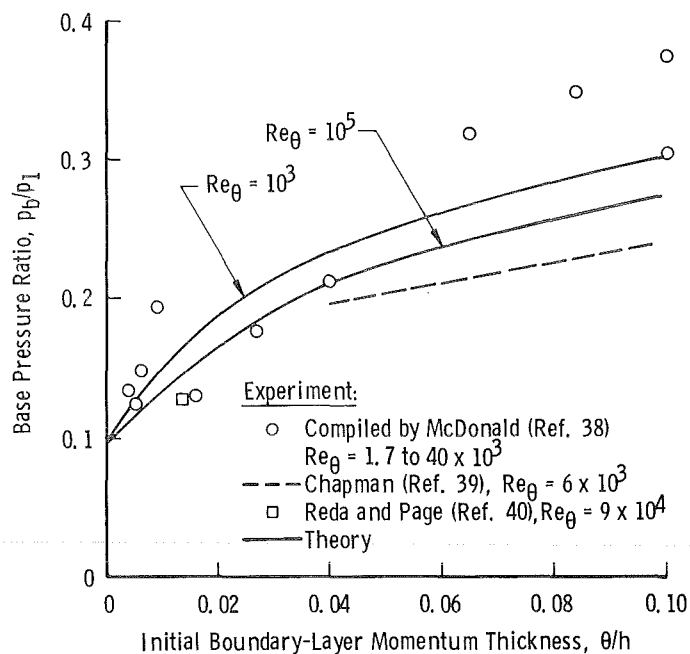


Figure 18. Effect of the initial boundary layer on the base pressure in planar flow ($M_{a1} = 3.0$).

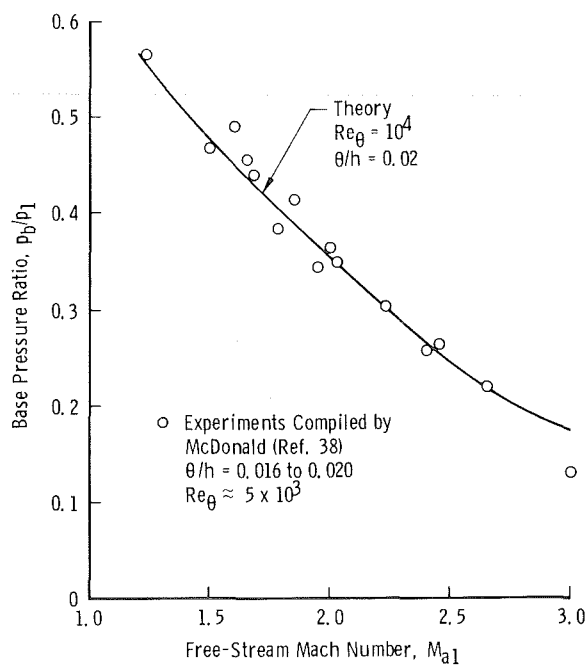
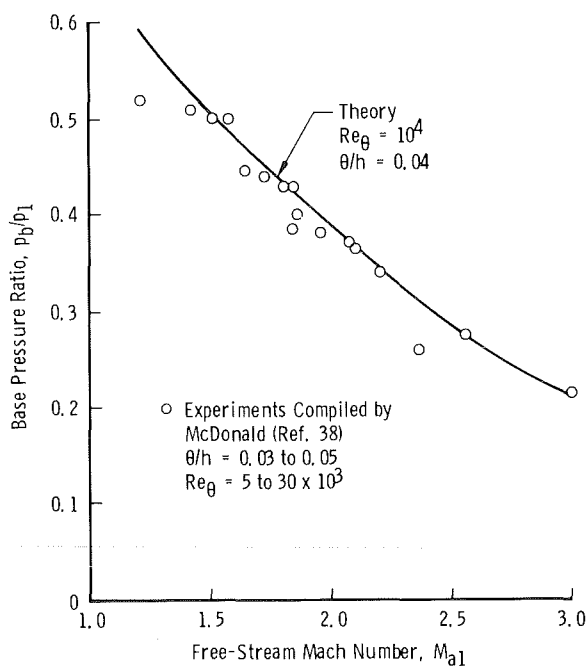
a. $\theta/h = 0.02$ b. $\theta/h = 0.04$

Figure 19. Mach number effect on the base pressure for planar flow.

Most near-wake flows of engineering interest involve initial boundary layers of moderate thickness, with θ/h values less than 0.05. The base pressure predictions of the present analysis for this range of θ/h are shown in Fig. 20 for M_{a1} from 1.2 to 4.0. Also shown in Fig. 20 are the predictions of the Korst theory for no initial boundary layer. Because of a fortunate combination of physically unrealistic assumptions, this simplest version of the Korst theory provides fairly satisfactory predictions of planar base pressure in the range of initial boundary layers most often encountered in engineering applications.

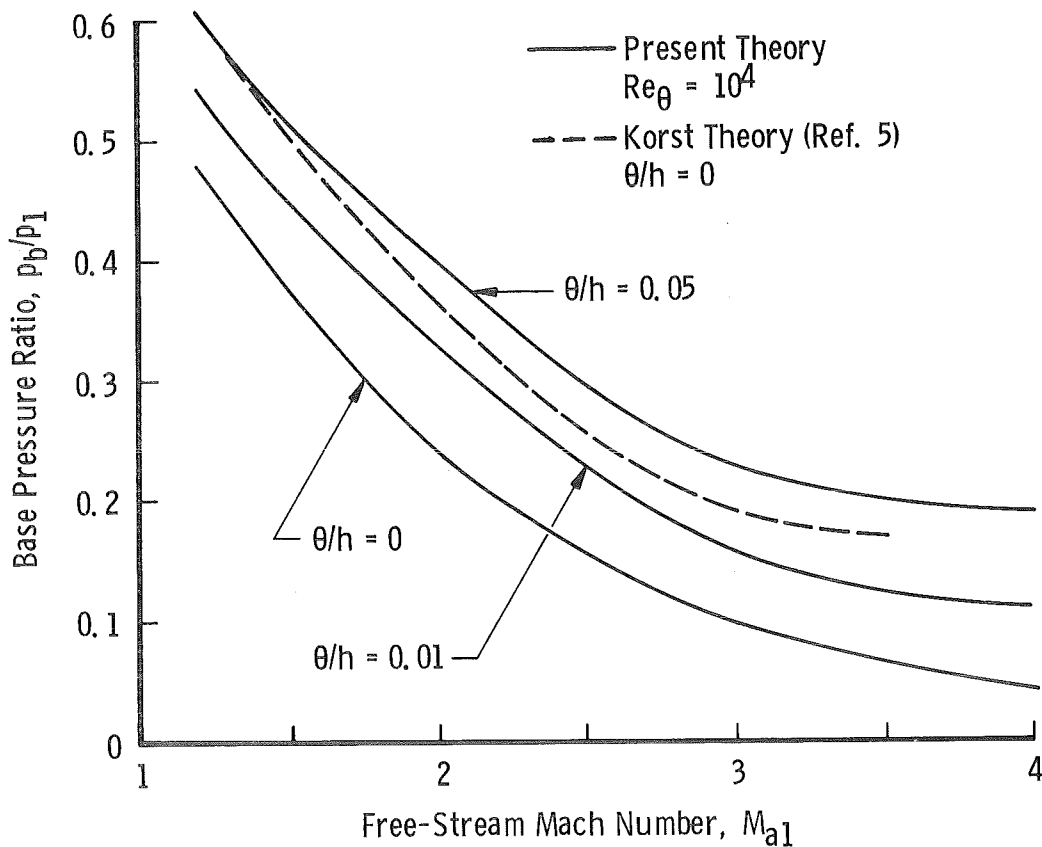


Figure 20. Predicted base pressure for planar flow.

3.3 PLANAR FLOW-FIELD STRUCTURE

Predicted axial distributions of the total pressure at the supersonic edge of the turbulent shear layer are shown in Fig. 21 for three typical planar wake flows. A value of p_{os}/p_{oa} less than unity indicates that the shear layer is growing into the rotational remnant of the initial boundary layer, and the point at which p_{os}/p_{oa} becomes unity is

the point where the initial boundary-layer flow has been completely entrained. The results shown in Fig. 21 indicate that, even for relatively thin initial boundary layers ($\theta/h = 0.013 - 0.014$), the entire viscous near-wake structure downstream to the critical point is immersed in a rotational external flow.

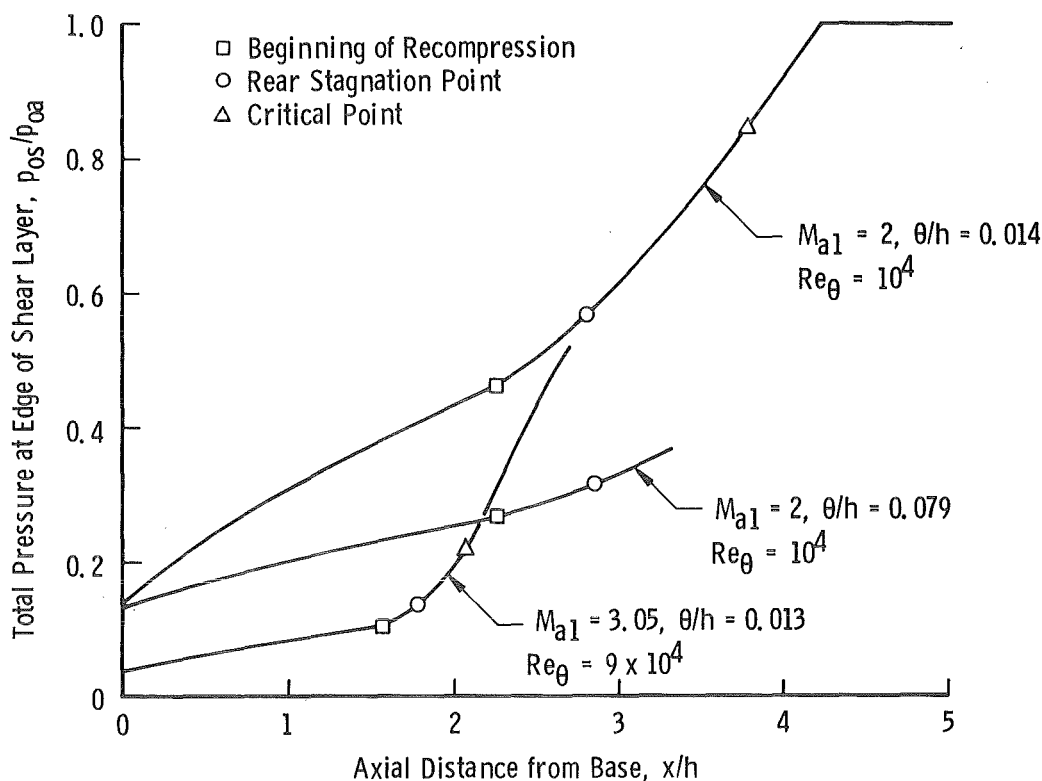


Figure 21. Total pressure at the edge of the shear layer for planar flow.

Predicted and experimental centerline (wall) static pressure distributions are shown in Fig. 22 for $M_{a1} = 2.0$. The distance to the beginning of recompression is somewhat overpredicted by the present theory; however, the complete predicted pressure distribution is considered to be in satisfactory agreement with the experiment, as is the predicted location of the RSP. The critical point in this flow occurs at a centerline Mach number of 0.64.

The predicted pressure distribution of Chow and Spring, which is shown in Fig. 22, is fairly satisfactory. Their analysis is carried out in two parts: (1) for the recompression process up to the RSP and (2) for the redeveloping flow downstream of the RSP. As shown, the two segments of the predicted pressure distribution do not join smoothly at the RSP.

The experimental centerline (wall) static pressure distribution obtained by Reda and Page (Ref. 40) for $M_{a1} = 3.05$ is shown in Fig. 23, along with the predicted pressure distribution. The overprediction of the distance to the onset of recompression is somewhat greater than at $M_{a1} = 2.0$; however, the axial distance to the experimental RSP is predicted to within ten percent. The centerline Mach number distribution for the Reda and Page flow is shown in Fig. 24. As a result of neglecting the streamwise transport terms in the viscous wake flow, the predicted centerline Mach number distribution always exhibits the sharp minimum at the beginning of recirculation. However, the solution seems to recover from this localized unrealistic behavior, and the downstream portion of the predicted M_c distribution is reasonably good. Detailed lateral profiles of the pitot pressure in the Reda and Page flow are shown in Fig. 25 for four axial stations; the first two stations are upstream of recompression, and the last two are downstream of the point where the wake flow is completely supersonic. The overall shapes of the predicted profiles agree fairly well with the experiment, but it is evident that the experimental shear layer growth rate in the wake regime is underpredicted. Part of the deviation between prediction and experiment at the two downstream stations may be attributed to the presence of the strong recompression shock wave, which is treated as an isentropic compression in the analysis.

The "brute force" technique described in Section 2.11 was used to obtain the planar flow-field solutions which extend through the critical region.

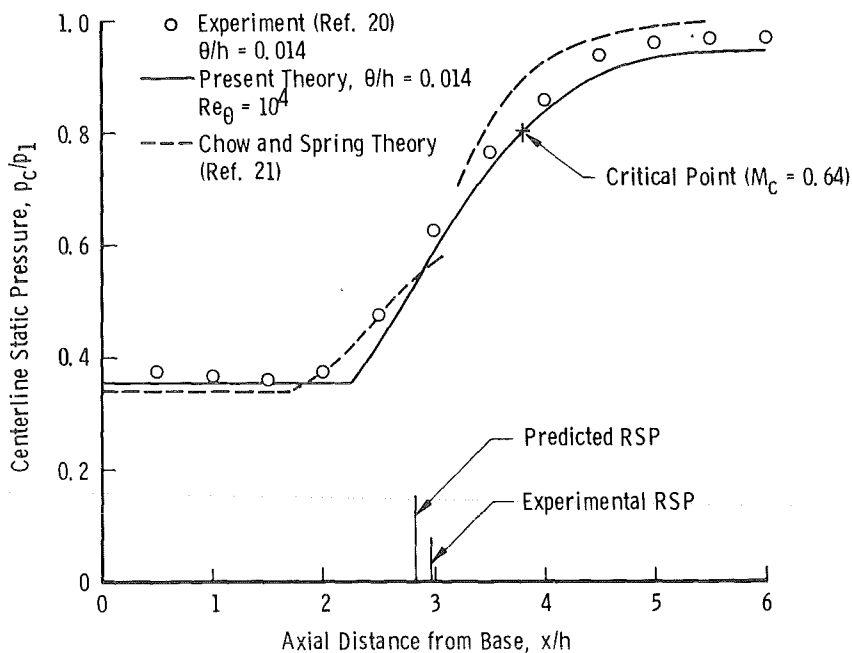


Figure 22. Centerline pressure distribution for planar wake flow ($M_{a1} = 2.0$).

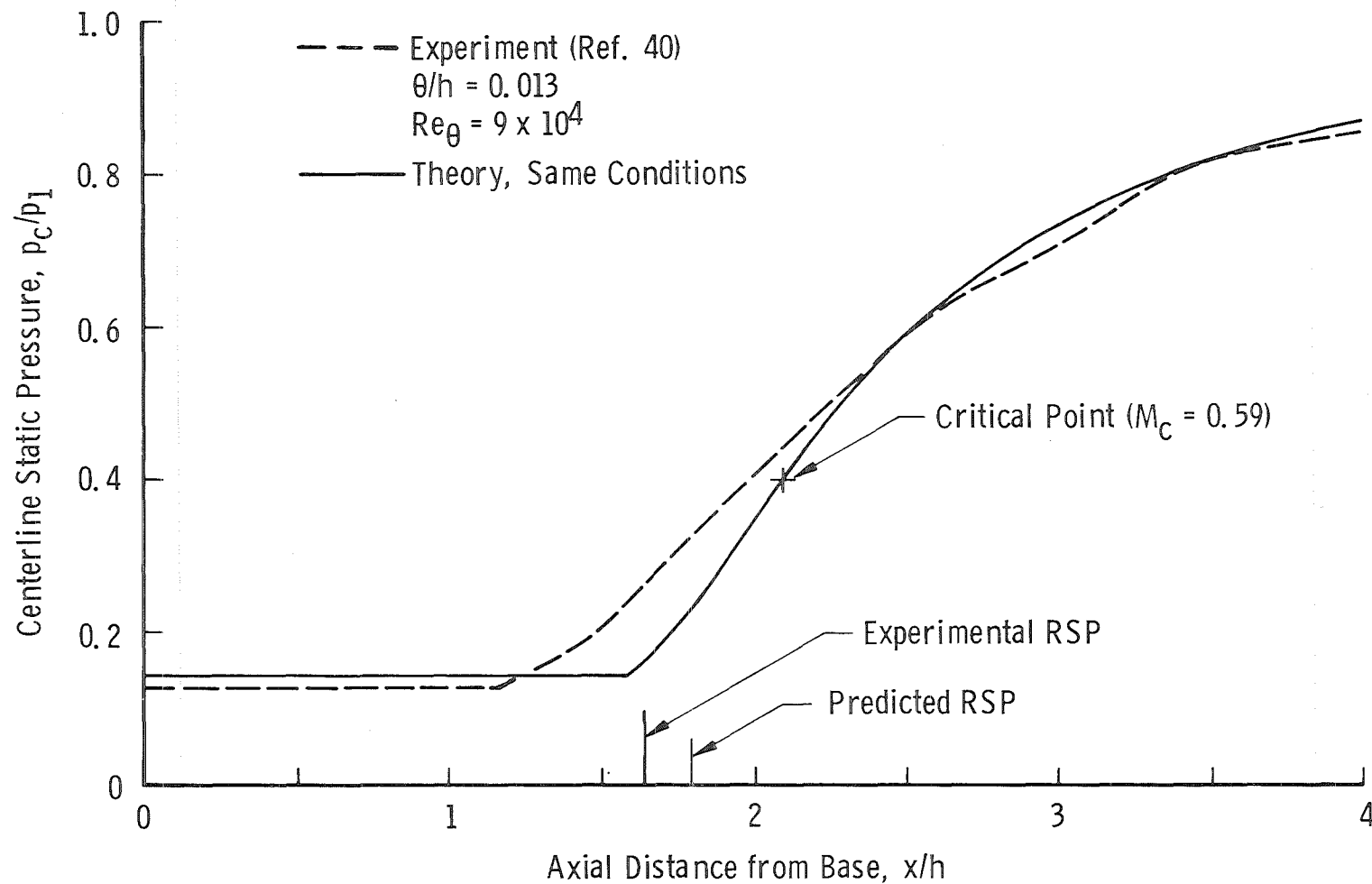


Figure 23. Centerline pressure distribution for planar wake flow ($M_{a1} = 3.05$).

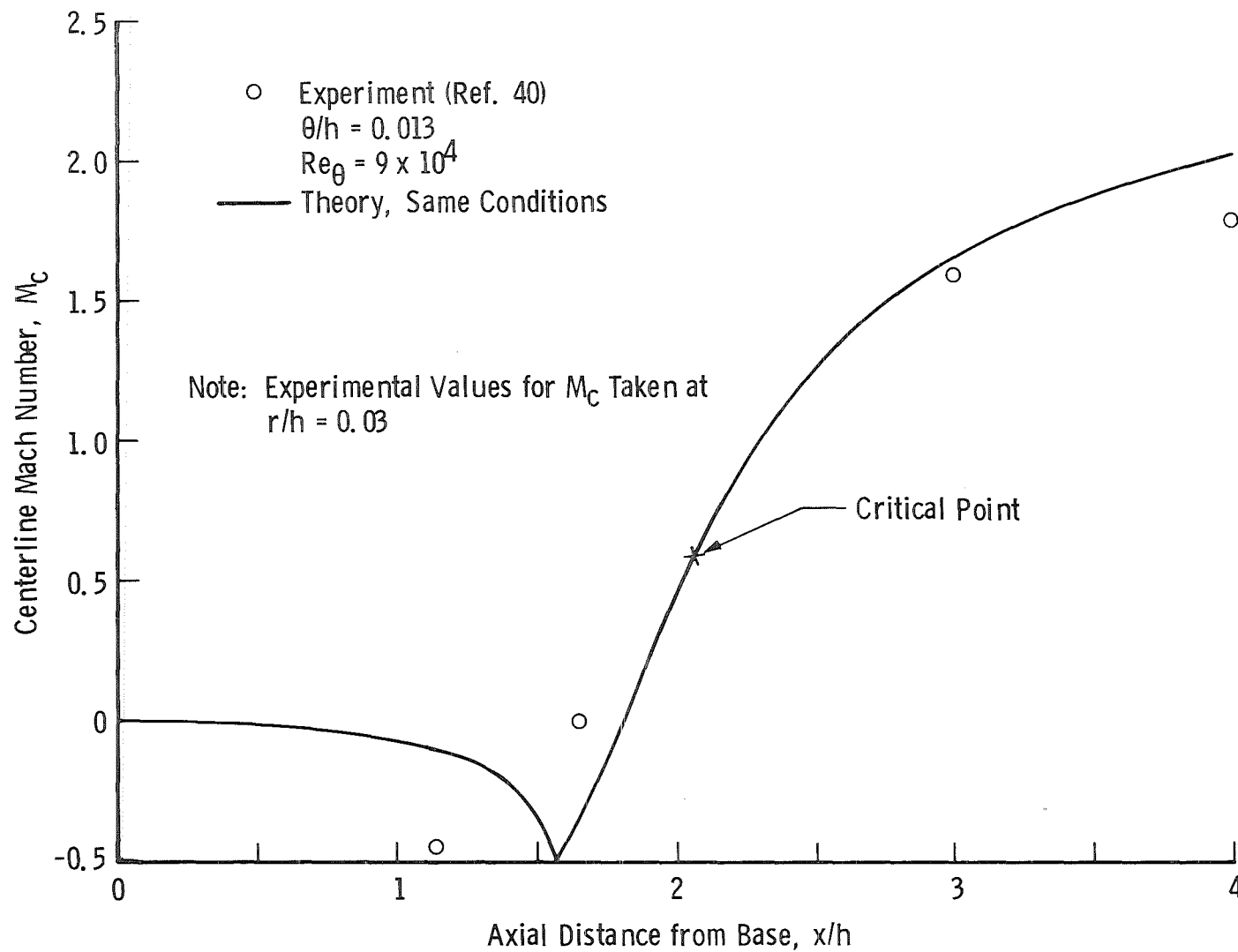


Figure 24. Centerline Mach number distribution for planar wake flow ($M_{a1} = 3.05$).

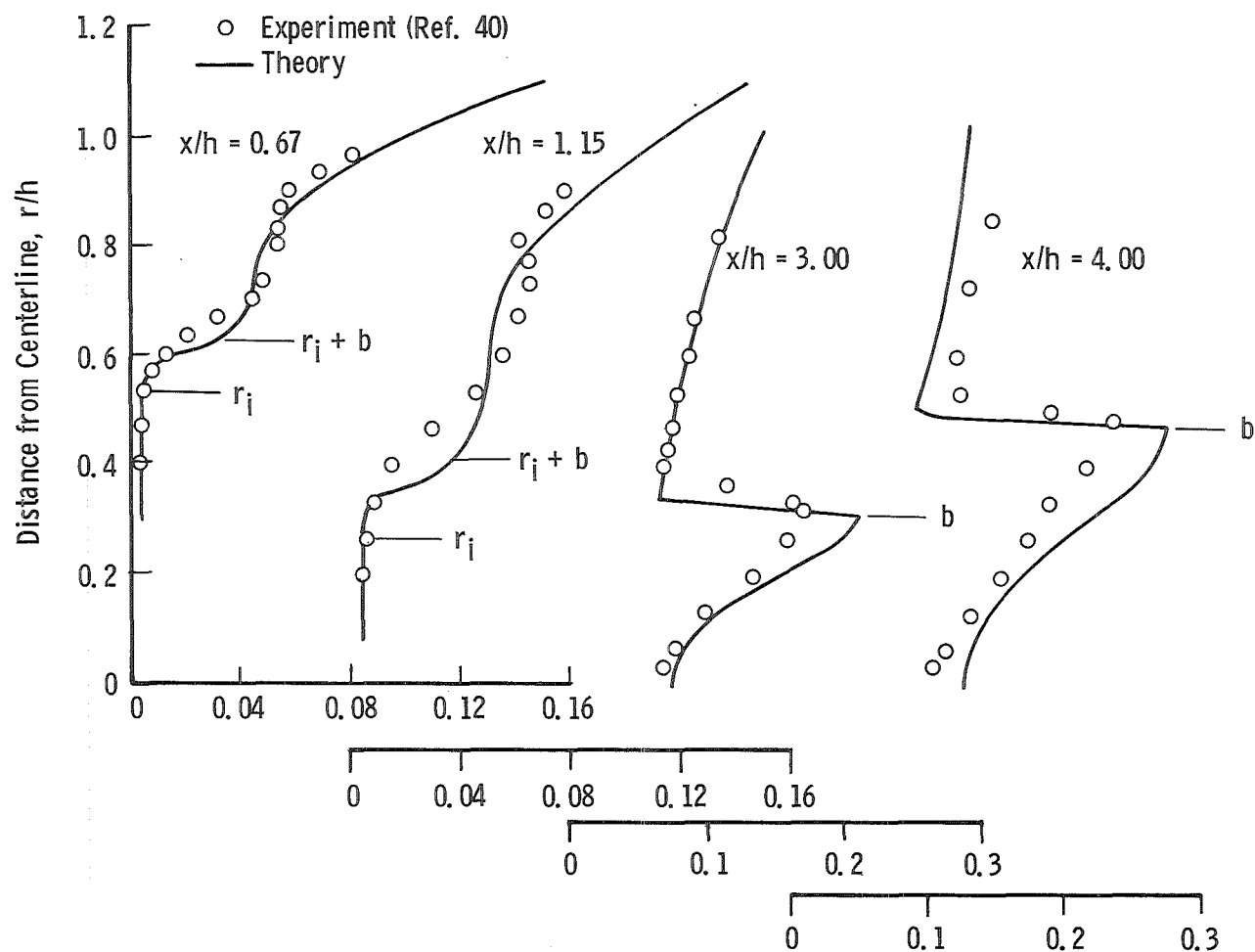


Figure 25. Pitot pressure profiles for planar wake flow ($M_{a1} = 3.05$).

3.4 AXISYMMETRIC BASE PRESSURE

In order to avoid possible support interference effects on the base pressure data, results from experiments without base stings (free flight or annular tunnel experiments) have been used for comparison with the present analytical model. The effect of initial boundary-layer momentum thickness on the base pressure is shown in Fig. 26 for $M_{a1} = 2.0$. As was found for planar flows, the predicted axisymmetric base pressure at $M_{a1} = 2.0$ is insensitive to changes in Re_θ in the range from 10^3 to 10^5 . Although the experimental base pressures are predicted with less than ten-percent error, the analytical results exhibit a peculiar oscillation about the expected results, which are indicated by the dashed line. The oscillation is attributed to the R_T model used in the reattachment region, which is overly sensitive to small changes in the flow field. The R_T model yields realistic results for higher Mach numbers, say 3.0 or 4.0, but the results at Mach numbers less than 2.0 exhibit more oscillation than shown in Fig. 26.

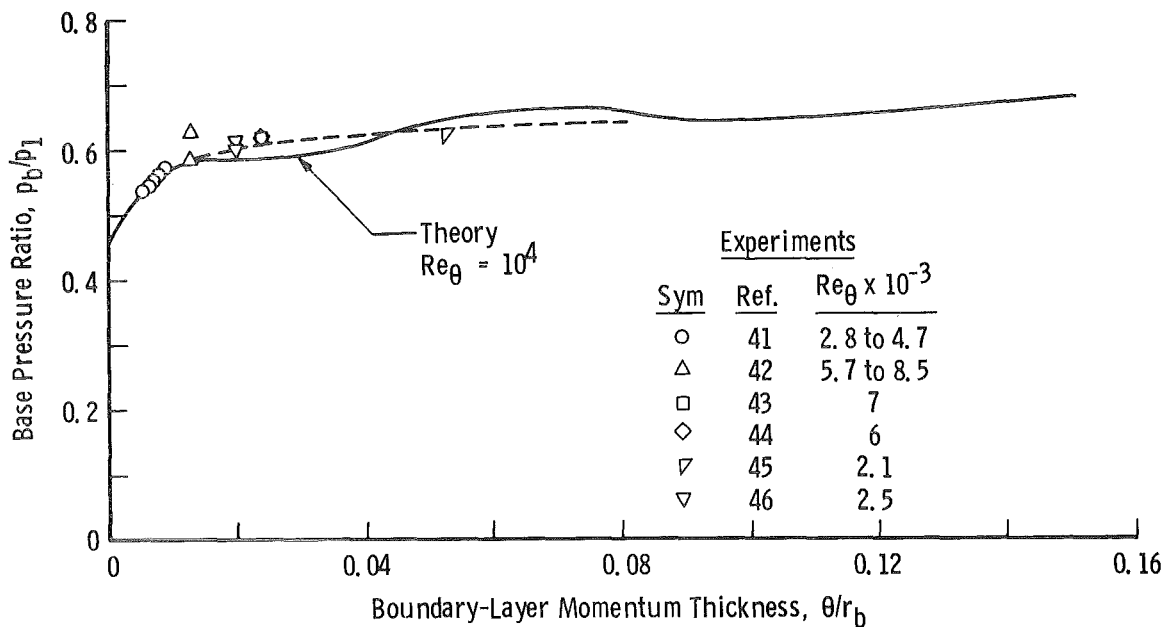


Figure 26. Effect of the initial boundary layer on the base pressure in axisymmetric flow ($M_{a1} = 2.0$).

The effect of initial boundary-layer momentum thickness on the base pressure is shown in Fig. 27 for $M_{a1} = 3.9$; the prediction is reasonably satisfactory.

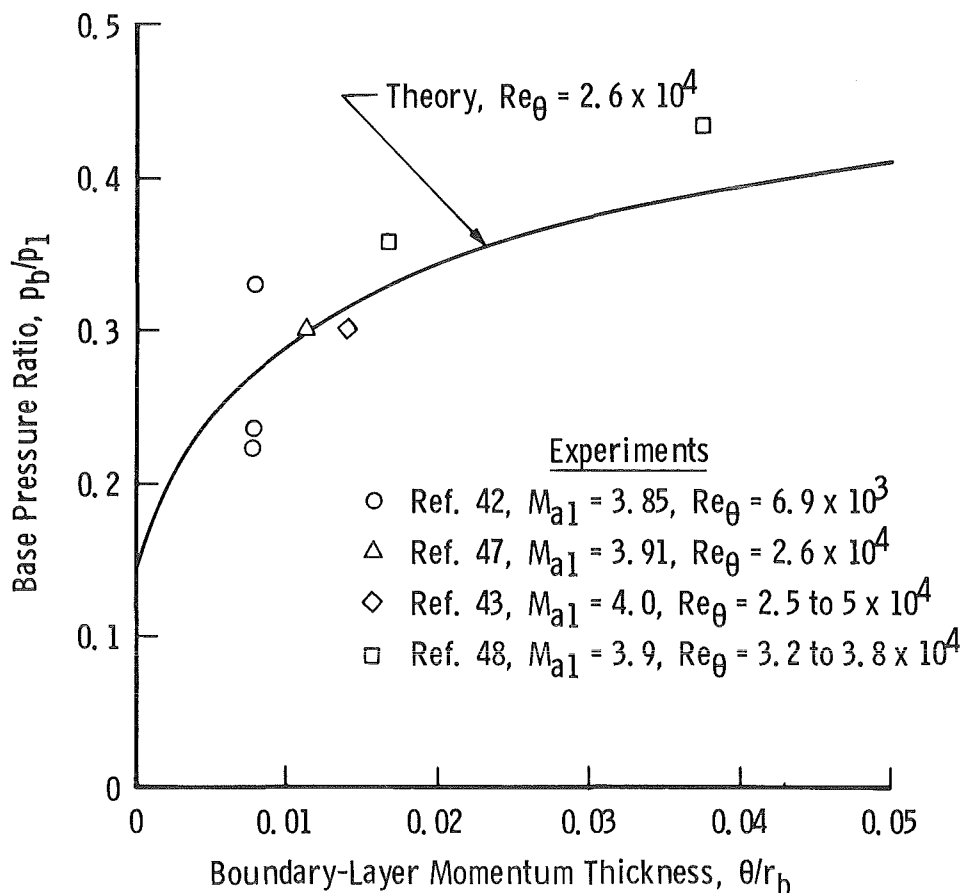


Figure 27. Effect of the initial boundary layer on the base pressure in axisymmetric flow ($M_{a1} = 3.9$).

The effect of free-stream Mach number on the axisymmetric base pressure is shown in Fig. 28. In view of the considerable scatter in the experimental data, the predictions for $\theta/r_b = 0.01$ and $\theta/r_b = 0.05$ are considered to be satisfactory for M_{a1} greater than 2.0. However, at lower Mach numbers the peculiarities caused by the R_T model are evident. The prediction for $\theta/r_b = 0.01$ is realistic down to a Mach number of 1.5, below which the base pressure ratio is predicted to be constant. A similar flattening of the p_b/p_1 curve for $\theta/r_b = 0.05$ occurs at Mach numbers less than 2.0. Because of the unrealistic behavior of the recompression region turbulent transport model, the near-wake analysis in its present form is not recommended for use at free-stream Mach numbers less than about 1.7.

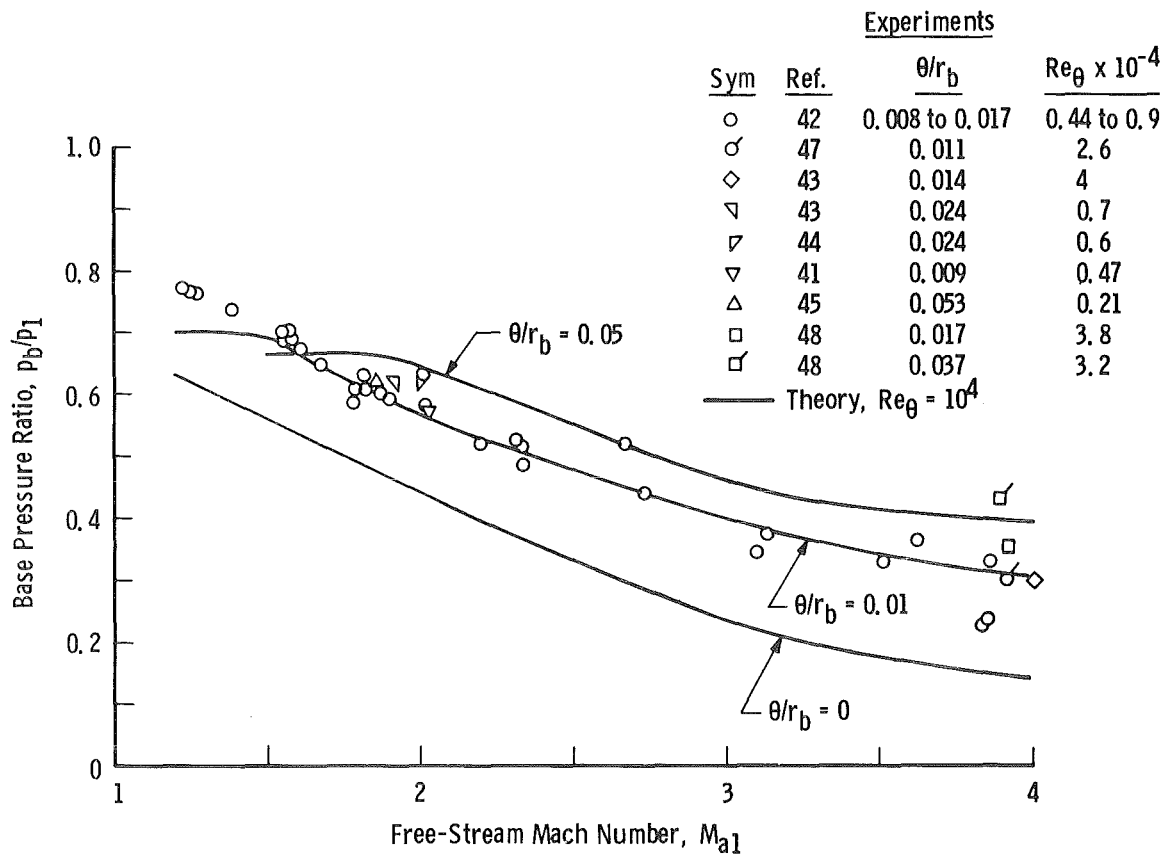


Figure 28. Mach number effect on the base pressure for axisymmetric flow.

3.5 EFFECT OF BASE BLEED ON AXISYMMETRIC BASE PRESSURE

Results of the axisymmetric base bleed experiments of Sirieix, et al. (Ref. 43), are shown in Fig. 29, along with the predictions of the near-wake analysis. The experimental trend of increasing base pressure with increasing base bleed flow is well predicted; in addition, the maximum difference between the predicted and experimental base pressures is less than eight percent.

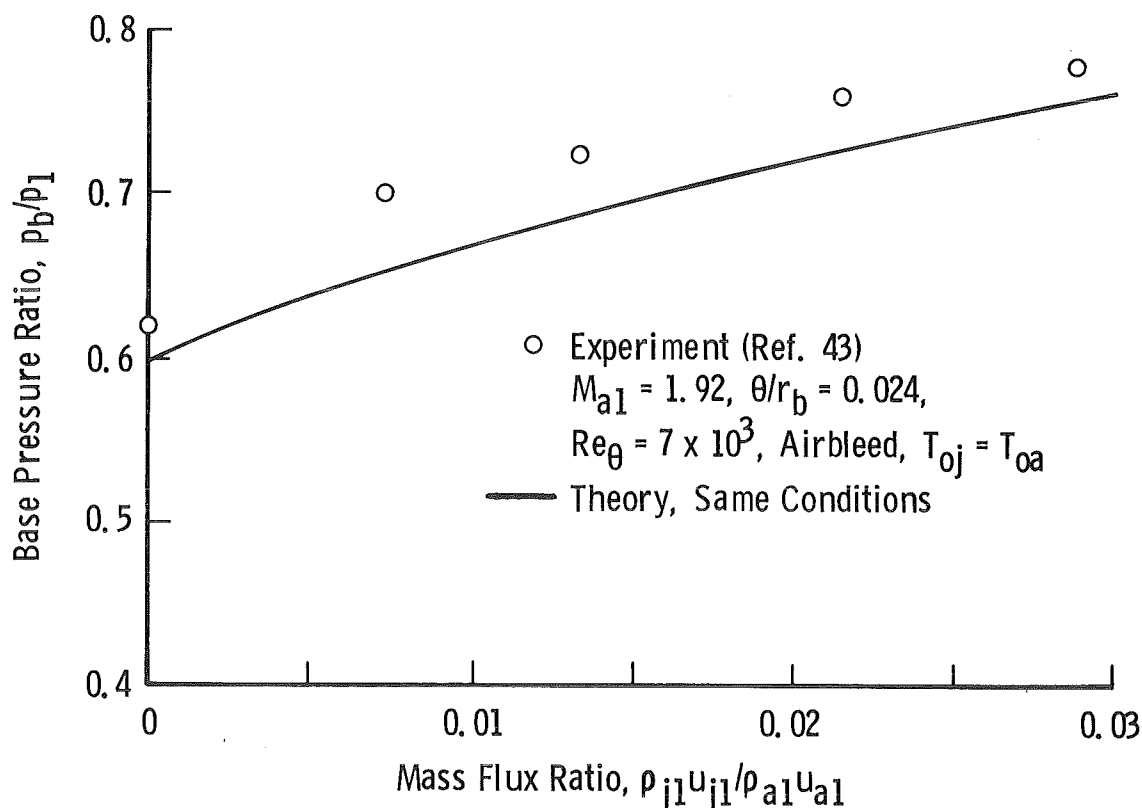


Figure 29. Effect of base bleed on axisymmetric base pressure.

3.6 AXISYMMETRIC FLOW-FIELD STRUCTURE

Predicted axial distributions of the total pressure at the supersonic edge of the turbulent shear layer are shown in Fig. 30 for three typical axisymmetric wake flows. As was found for planar flows, most or all of the viscous near-wake structure is imbedded in a rotational external flow. The abrupt increase in the slope of the p_{0s} versus x curves at the onset of recompression, which is much more pronounced for axisymmetric flow than for planar flow, indicates a sudden increase in the entrainment rate of the shear layer. The mass flow in the shear layer increases rapidly with distance in the recompression region, even though the thickness of the shear layer, b , initially decreases in this region; this phenomenon is related to the rapid change in the shear layer velocity profile during recompression.

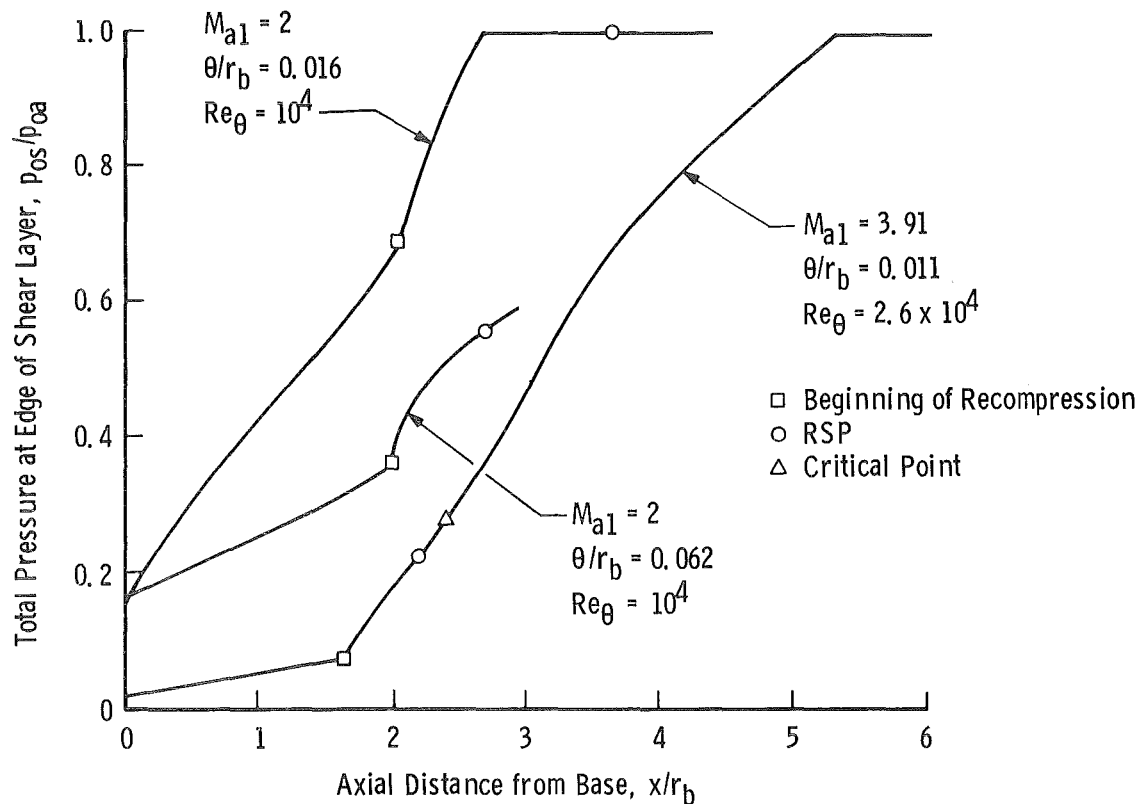


Figure 30. Total pressure at the edge of the shear layer for axisymmetric flow.

The experimental centerline static pressure distribution measured by Seiling, et al. (Ref. 47), for $M_{a1} = 3.91$ is shown in Fig. 31, along with the predictions of the near-wake analysis. The solution through the critical region was obtained with the "brute force" technique described in Section 2.11. The distance to the onset of recompression is overpredicted as is the distance to the RSP. The characteristic overshoot of the static pressure is predicted.

The length scale of the near wake, as indicated by the distance to the onset of recompression, is strongly influenced in high Mach number flows by the rotational boundary-layer flow at the base plane. To illustrate this point, a computation of the flow field of Seiling, et al., was made with the assumption that there was no initial boundary layer, i.e., that the turning of the flow at the base plane corresponds to a Prandtl-Meyer expansion of the inviscid free stream through the pressure ratio p_b/p_1 . The results, which are presented in Fig. 31, show that the distance to the onset of recompression is nearly twice as large as that predicted when the initial boundary layer is included.

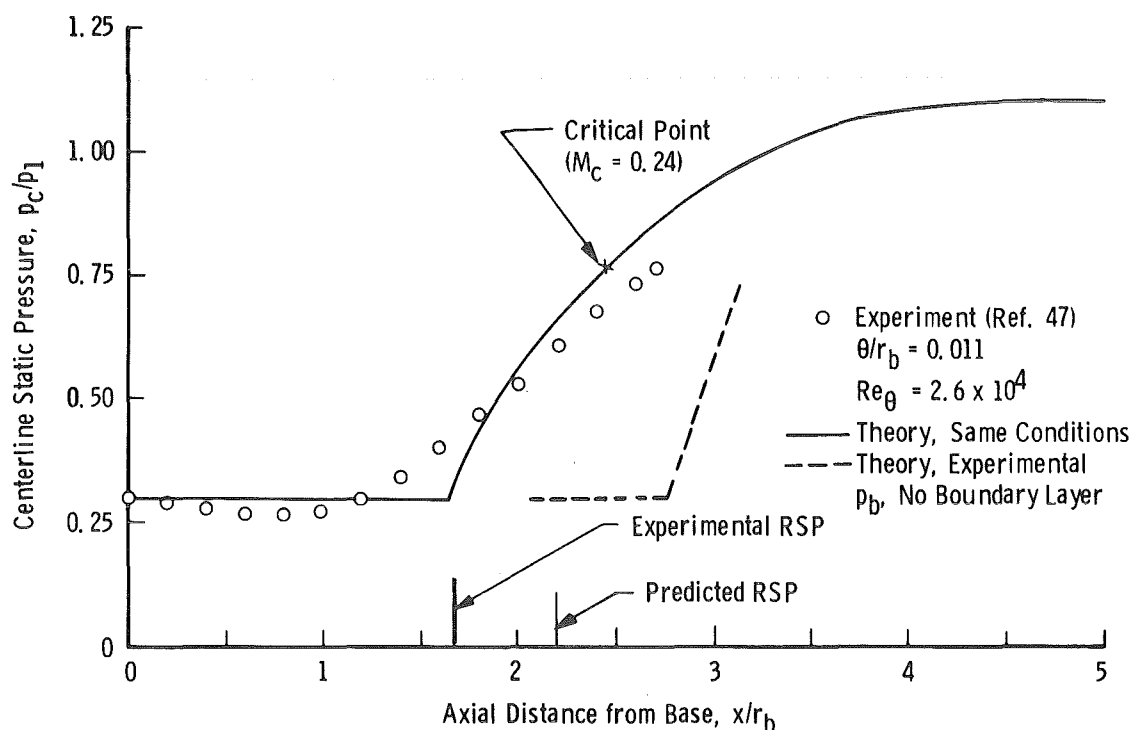


Figure 31. Centerline pressure distribution for axisymmetric wake flow ($M_{a1} = 3.91$).

Detailed radial profiles of pitot pressure, which were measured by Seiling, et al., are shown in Fig. 32. The predicted profiles agree well with the experiment, although the experimental shear layer growth rate in the wake regime is underpredicted; a similar result was found for planar flow (Fig. 25). Based on the results shown in Fig. 32, as well as those shown in Fig. 25 for planar flow, it does not appear that the neglect of the finite-strength lip shock is a serious deficiency in the present analysis, even for free-stream Mach numbers up to 4.0.

The experimental centerline pressure distribution measured by Sirieix, et al. (Ref. 43), for $M_{a1} = 1.92$ is shown in Fig. 33. For Mach numbers in the neighborhood of 2.0, the "brute force" technique for obtaining the solution through the critical region is unsuccessful, so the extrapolation technique described in Section 2.11 was used to obtain the solution shown in Fig. 33. The distance to the onset of recompression is somewhat overpredicted, and the distance to the RSP is overpredicted by 25 percent. An unusual inflection in the centerline pressure distribution is predicted in the region of the RSP, but the characteristic overshoot in the pressure distribution is preserved in the solution.

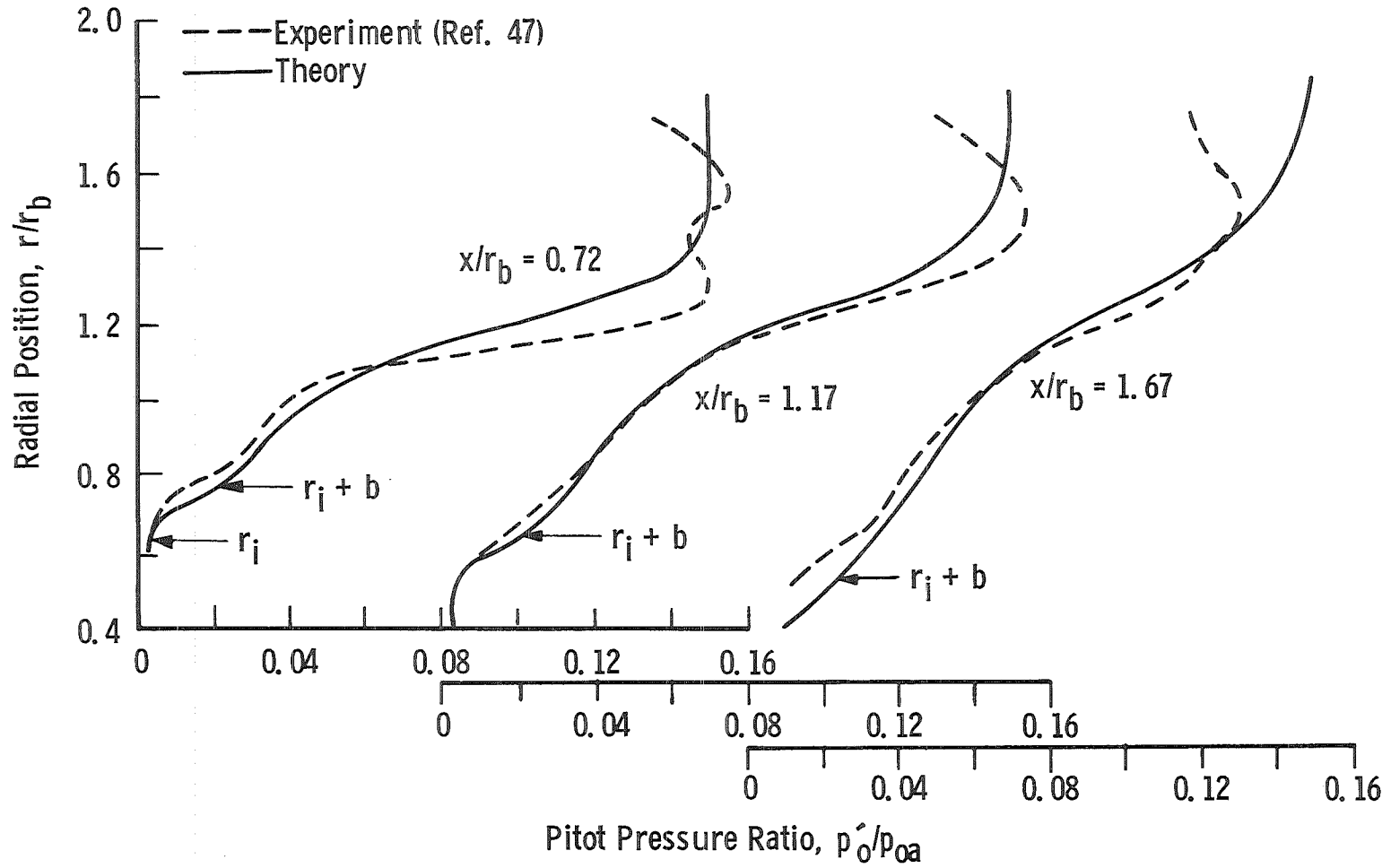


Figure 32. Pitot pressure profiles for axisymmetric wake flow ($M_{a1} = 3.91$).

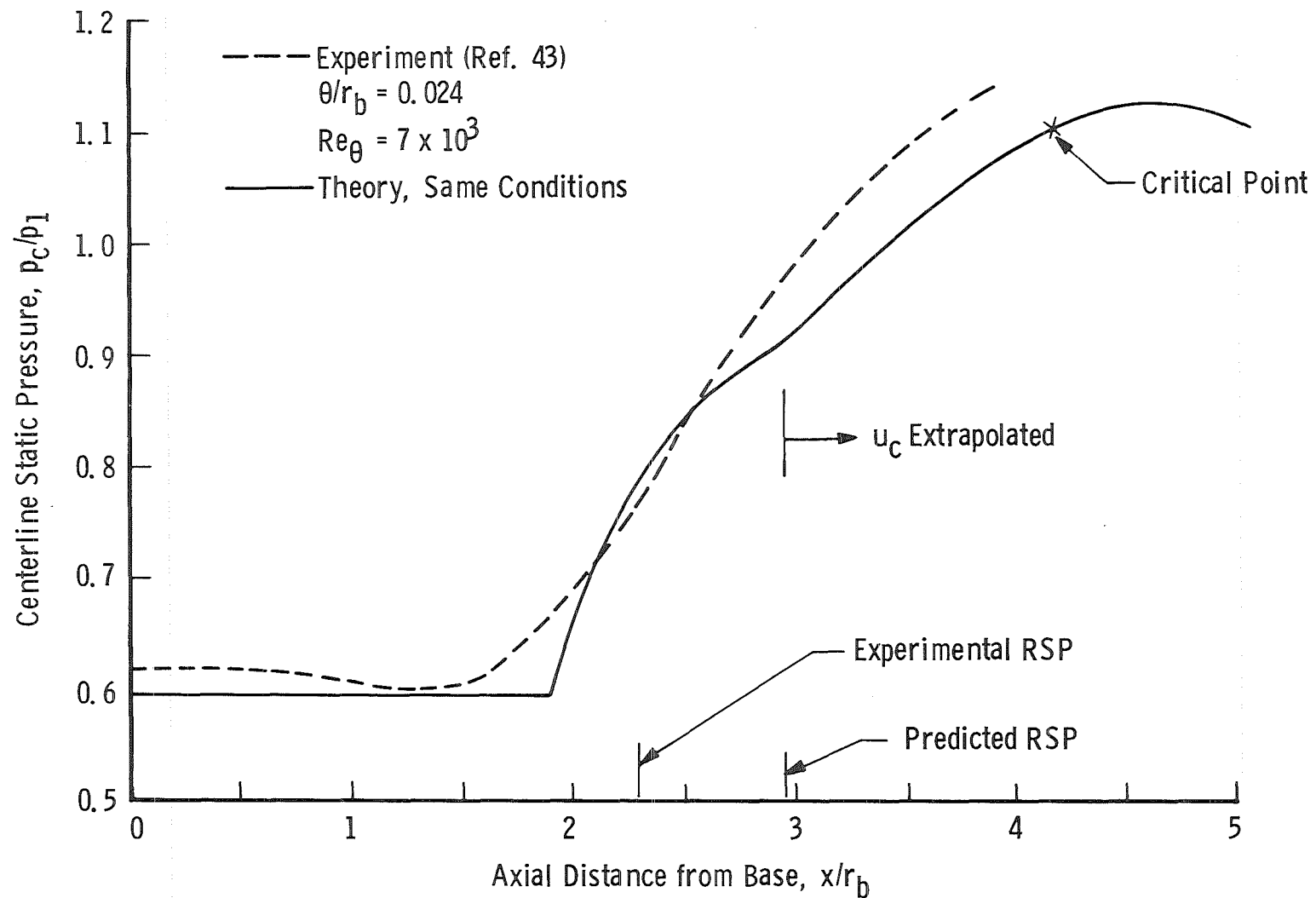


Figure 33. Centerline pressure distribution for axisymmetric wake flow ($M_{a1} = 1.92$).

The centerline Mach number distribution for the flow of Sirieix, et al., is shown in Fig. 34. As was shown for planar flow, the predicted Mach number distribution has a sharp minimum; this unrealistic behavior is localized, and the slope of the predicted centerline Mach number distribution agrees well with the experiment at the RSP, although the entire distribution is shifted downstream from the experimental distribution by the same distance as the RSP shift.

The experimental centerline pressure distribution measured by Reid and Hastings for $M_{a1} = 2.03$ is shown in Fig. 35. The inflection shown in Fig. 33 does not appear in this solution, which was also obtained with the centerline velocity extrapolation technique.

Based on the results shown in Figs. 33 through 35, it can be concluded that the extrapolation technique for obtaining solutions through the critical region is reasonably successful.

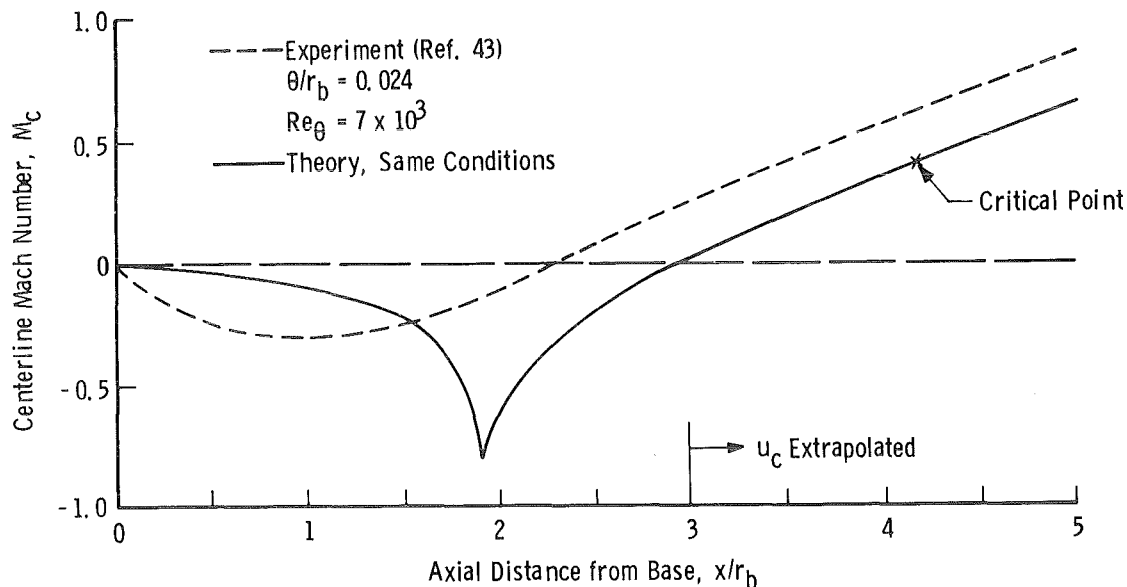


Figure 34. Centerline Mach number distribution for axisymmetric wake flow ($M_{a1} = 1.92$).

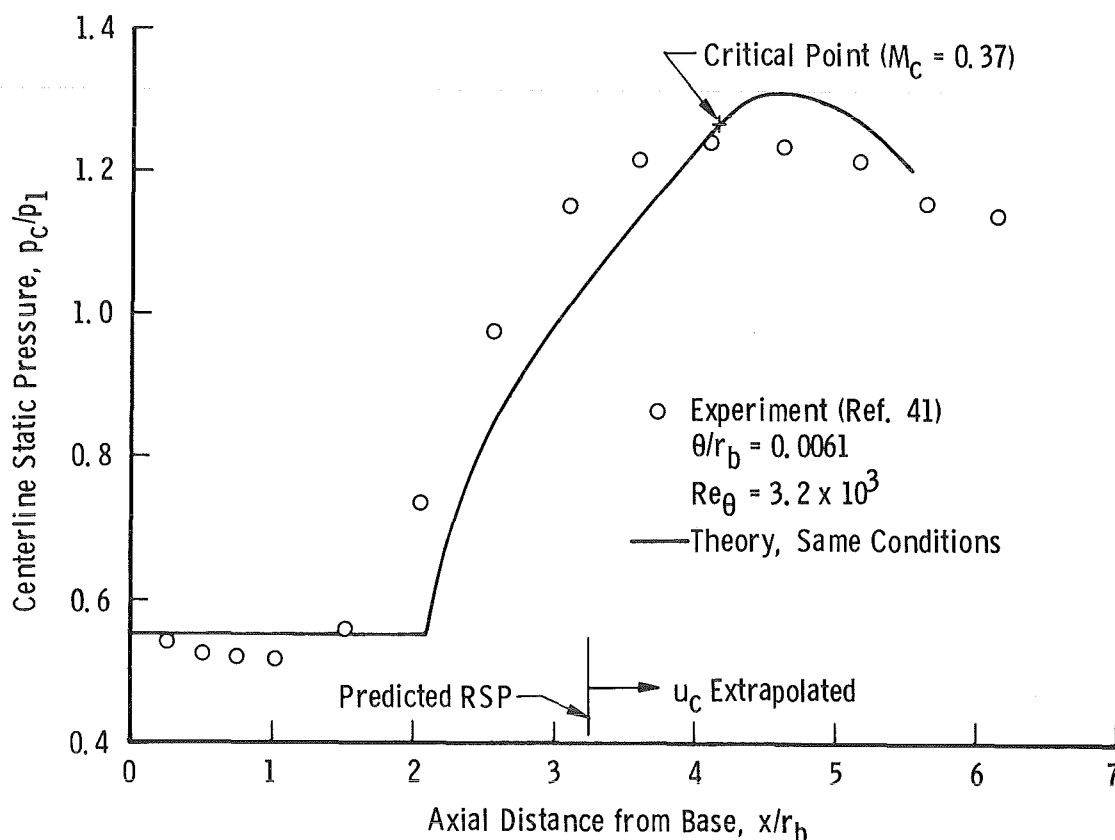


Figure 35. Centerline pressure distribution for axisymmetric wake flow ($M_{a1} = 2.03$).

3.7 DIVIDING STREAMLINE PROPERTIES

Although dividing streamline concepts play no role in the present near-wake analysis, the location of this streamline and its velocity are computed. Predicted distributions of total pressure on the dividing streamline are shown in Fig. 36 for three typical planar flows. Somewhat surprisingly, the predicted dividing streamline total pressure remains nearly constant from the base plane to the RSP.

The simple Korst theory for no initial boundary layer yields base pressure results which are similar to those of the present analysis for θ/h from 0.01 to 0.05 (Fig. 20). Korst's theory is based on three fundamental assumptions: (1) an isentropic recompression along the dividing streamline, (2) stagnation of the dividing streamline at the peak of the recompression pressure rise, and (3) negligible reverse flow velocities. According to the results shown in Fig. 36, the first assumption is a good one for planar flows. It has long been known that the dividing streamline does not stagnate at the peak of the pressure rise, i.e., the RSP occurs at a station where the pressure is much less than

the peak value (Figs. 22 and 23). But Korst's assumption of negligible reverse flow velocities leads to overprediction of the dividing streamline total pressure (Fig. 36). This high total pressure in Korst's analysis, combined with the unrealistically high pressure at which the dividing streamline is assumed to stagnate, leads to base pressure predictions which are about correct.

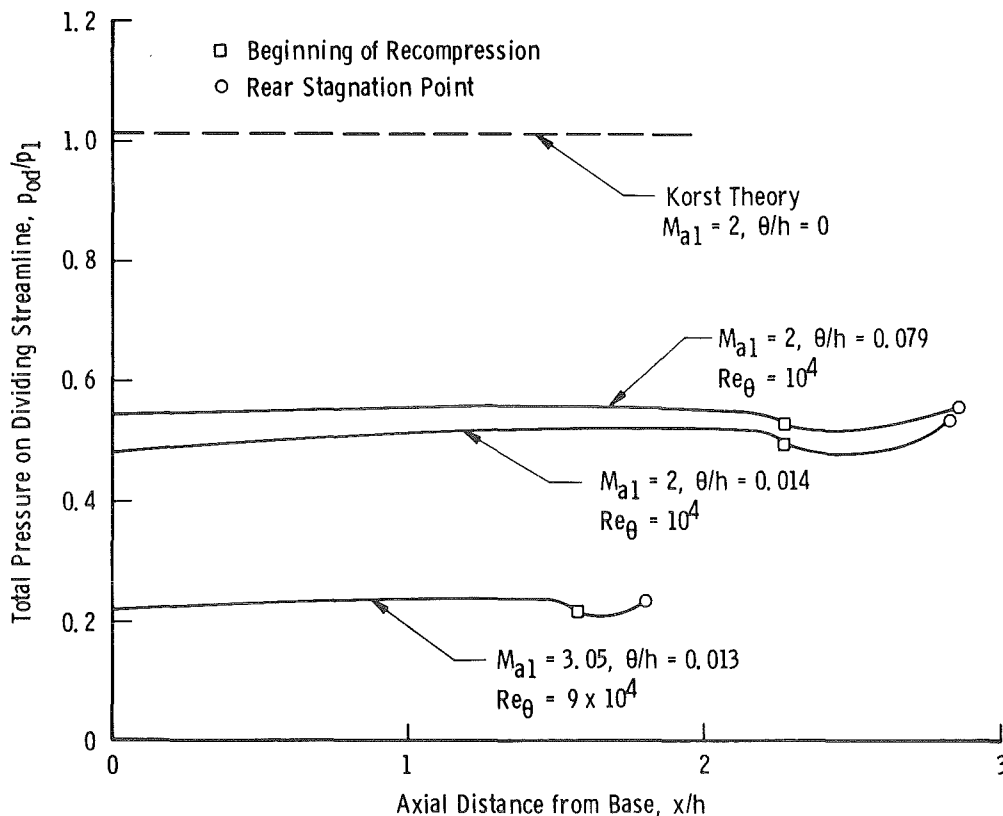


Figure 36. Total pressure along the dividing streamline for planar flows.

Predicted distributions of the total pressure on the dividing streamline are shown in Fig. 37 for three typical axisymmetric wake flows. In contrast to the results for planar flows, the dividing streamline total pressure is predicted to increase significantly during the recompression process. However, the quality of the detailed predictions of the present model for axisymmetric reattaching flows is not considered to be good enough so that strong conclusions can be drawn about the validity of isentropic recompression of the dividing streamline.

One point is clear from the results discussed in this section: any wake analysis which is based on dividing streamline concepts (e.g., Ref. 21) should include the effect of finite reverse flow velocities on the dividing streamline properties.

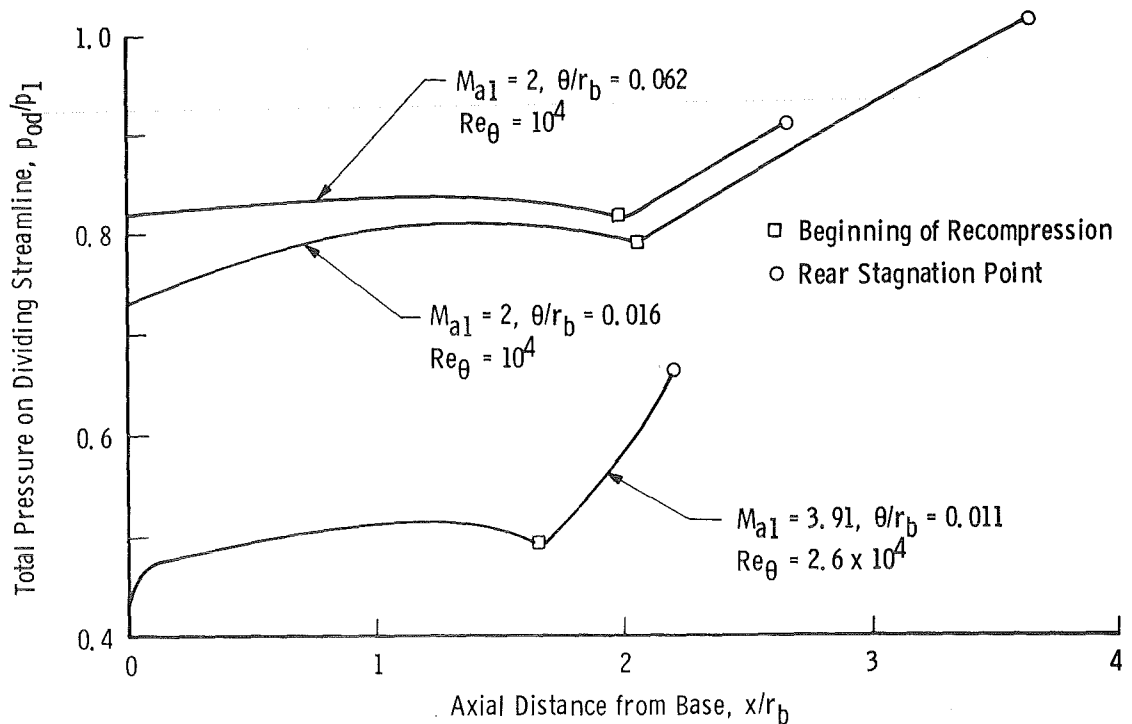


Figure 37. Total pressure along the dividing streamline for axisymmetric flows.

4.0 CONCLUDING REMARKS

The correlations of the present near-wake analysis with a variety of planar and axisymmetric experiments indicate that the overall framework of the analysis is physically realistic. Because both the detailed flow-field structure and the base pressure can be predicted reasonably well, it can be concluded that the arbitrariness in the selected turbulent transport model is not used to mask the effect of physically unrealistic aspects of the analysis. The method of computing the inviscid remnant of the initial boundary layer is considered to be a very important feature of the analysis, as is the inclusion of finite reverse flow velocities.

In any analysis of turbulent flow, the selection of an adequate turbulent transport model is a major problem. The transport model used in the present analysis yields acceptable base pressure results for planar flows, but yields inconsistent results for axisymmetric flows with free-stream Mach numbers less than about 2.0. The concept of scaling the recompression region turbulent transport properties with the value of the turbulent Reynolds number at the rear stagnation point seems to be satisfactory. But the model used to relate this turbulent Reynolds number to the flow-field properties must be improved if adequate predictions of axisymmetric flows are to be obtained over the

entire supersonic Mach number range of practical interest. The correlations of the analytical results with the flow-field experiments of Reda and Page and of Seiling, et al., show that the turbulent mixing rate is somewhat underpredicted in the region upstream of recompression and indicate that the R_T model for this region should be improved. However, based on limited numerical experimentation, it is not expected that an improved R_T model for the wake regime would greatly change the predicted base pressures; the predicted base pressure is much more strongly dependent on the turbulent transport properties in the recompression region than on those properties in the wake regime.

Because of the unresolved problems in the solution of the species conservation equations, the near-wake model as presently formulated cannot be used for flows in which the base bleed gas is different from the external stream gas. Many practical wake flows involve two gases; therefore, a major emphasis in future work on the near-wake model should be placed on developing a satisfactory technique for solving the species conservation equations.

Although the overall framework of the near-wake analysis seems to be physically realistic, the behavior of the solutions in the vicinity of the onset of recompression is not satisfactory. The length of the constant pressure region is overpredicted and an unrealistic sharp minimum in the centerline velocity is predicted. Both of these characteristics of the solution can probably be avoided by abandoning the assumption that the pressure is constant in the wake regime. In order to solve for the pressure distribution, however, an additional equation is required. A reasonable approach would be to add an axial momentum equation for the flow along the axis; this equation would include an approximate term to represent the streamwise turbulent transport of momentum.

Even though the present formulation of the near-wake model is deficient in several respects, the model provides a significant improvement in the capability to analyze supersonic turbulent near-wake flows. Indeed, the present model for axisymmetric flows without base stings is the first to realistically include the effect of the initial boundary-layer thickness and shape and the effects of base bleed.

REFERENCES

1. Strahle, W. C. "Theoretical Consideration of Combustion Effects on Base Pressure in Supersonic Flight." Twelfth Symposium (International) on Combustion, The Combustion Institute, Pittsburgh, 1969, pp. 1163-1173.
2. Wasson, R. A., Jr. and Darlington, C. R. "Performance of an External Burning Rocket Configuration in a Supersonic Flight Environment." AEDC-TR-75-102 (ADB005762L), July 1975.

3. Crocco, L. and Lees, L. "A Mixing Theory for the Interaction between Dissipative Flows and Nearly Isentropic Streams." Journal of the Aeronautical Sciences, Vol. 19, October 1952, pp. 649-676.
4. Korst, H. H. "A Theory for Base Pressures in Transonic and Supersonic Flow." Journal of Applied Mechanics, Vol. 23, December 1956, pp. 593-600.
5. Korst, H. H., Chow, W. L., and Zumwalt, G. W. "Research on Transonic and Supersonic Flow of a Real Fluid at Abrupt Increases in Cross Section - Final Report." ME Technical Report 392-5, University of Illinois, December 1959.
6. Alber, I. E. "Integral Theory for Turbulent Base Flows at Subsonic and Supersonic Speeds." Ph.D. Thesis, California Institute of Technology, June 1967.
7. Alber, I. E. and Lees, L. "Integral Theory for Supersonic Turbulent Base Flows." AIAA Journal, Vol. 6, No. 7, July 1968, pp. 1343-1351.
8. Strahle, W. C. and Mehta, G. "Turbulent Axisymmetric Base Flow Studies for External Burning Propulsion." in 11th JANNAF Combustion Meeting, Vol. II, CPIA Publication 261, December 1974, pp. 441-448.
9. Strahle, W. C., et al. "Turbulent Axisymmetric Base Flow Studies for External Burning Propulsion." Paper Presented at 12th JANNAF Combustor Meeting, Newport, Rhode Island, August 1975.
10. Davis, L. R. "Experimental and Theoretical Determination of Flow Properties in a Reacting Near Wake." AIAA Journal, Vol. 6, No. 5, May 1968, pp. 843-847.
11. Nash, J. F. "An Analysis of Two-Dimensional Base Flow including the Effect of the Approaching Boundary Layer." National Physical Laboratory Aero. Report 1036, July 1972.
12. Lamb, J. P and Hood, C. G. "An Integral Analysis of Turbulent Reattachment Applied to Plane Supersonic Base Flows." Transactions of the ASME, Series C, Vol. 90, 1968, pp. 553-560.
13. Hill, W. G. and Page, R. H. "Initial Development of Turbulent Compressible Free Shear Layers." Journal of Basic Engineering, Vol. 91, 1969, pp. 67-73.
14. Lewis, J. E. and Behrens, W. "Fluctuation Measurements in the Near Wake of a Wedge with and without Base Injection." AIAA Journal, Vol. 7, No. 4, April 1969, pp. 664-670.

15. Page, R. H. and Sernas, V. "Apparent Reverse Transition in an Expansion Fan." AIAA Journal, Vol. 8, No. 1, January 1970, pp. 189-190.
16. Zumwalt, G. W. "Analytical and Experimental Study of the Axially-Symmetric Supersonic Base Pressure Problem." Ph.D. Dissertation, University of Illinois, 1959.
17. Mueller, T. J. "Determination of the Turbulent Base Pressure in Supersonic Axisymmetric Flow." Journal of Spacecraft and Rockets, Vol. 5, No. 1, January 1968, pp. 101-107.
18. McDonald, H. "Turbulent Shear Layer Reattachment with Special Emphasis on the Base Pressure Problem." Aeronautical Quarterly, Vol. XV, August 1964, p. 247.
19. McDonald, H. "An Analysis of the Turbulent Base Pressure Problem in Supersonic Axisymmetric Flow." Aeronautical Quarterly, Vol. XVI, May 1965, pp. 97-121.
20. Chow, W. L. "Recompression of a Two-Dimensional Supersonic Turbulent Free Shear Layer." Developments in Mechanics, Vol. 6, Proceedings of the Twelfth Midwestern Mechanics Conference, 1971, pp. 319-331.
21. Chow, W. L. and Spring, D. J. "Viscous Interaction of Flow Redevelopment after Flow Reattachment with Supersonic External Streams." AIAA Journal, Vol. 13, No. 12, December 1975, pp. 1576-1584.
22. Weng, C. H. "Base Pressure Problem Associated with Supersonic Axisymmetric External Flow Configurations." Ph.D. Dissertation, University of Illinois, 1975.
23. Weinbaum, S. "Rapid Expansion of a Supersonic Boundary Layer and Its Application to the Near Wake." AIAA Journal, Vol. 4, No. 2, February 1966, pp. 217-227.
24. Korst, H. H. "Dynamics and Thermodynamics of Separated Flows." in Heat and Mass Transfer in Boundary Layers, Volume 2, Edited by N. Afgan, et al., Pergamon Press, 1972, pp. 781-825.
25. Peters, C. E. "Turbulent Mixing and Burning of Coaxial Streams Inside a Duct of Arbitrary Shape." AEDC-TR-68-270 (AD680397), January 1969.
26. Peters, C. E., Phares, W. J., and Cunningham, T. H. M. "Theoretical and Experimental Studies of Ducted Mixing and Burning of Coaxial Streams." Journal of Spacecraft and Rockets, Vol. 6, No. 12, December 1969, pp. 1435-1441.

27. Green, J. E. "Two-Dimensional Turbulent Reattachment as a Boundary Layer Problem." in Separated Flows, Part 1, AGARD Conference Proceedings No. 4, May 1966, pp. 399-427.
28. Schubauer, G. B. and Tchen, C. M. "Turbulent Flow." in High Speed Aerodynamics and Jet Propulsion, Volume V, Turbulent Flows and Heat Transfer, Edited by C. C. Lin, Princeton University Press, 1959, p. 171.
29. Phares, W. J. and Loper, F. C. "A Technique for Solving Integro-Differential Equations with Application to Turbulent Mixing." AEDC-TR-64-209 (AD450730), November 1964.
30. Hama, F. R. "Experimental Investigations of Wedge Base Pressure and Lip Shock." NASA CR81031 and JPL/CIT TR-32-1003, December 1966.
31. Maise, G. and McDonald, H. "Mixing Length and Kinematic Eddy Viscosity in a Compressible Boundary Layer Flow." AIAA Journal, Vol. 6, No. 1, January 1968, pp. 73-80.
32. Tucker, M. "Approximate Calculation of Turbulent Boundary Layer Development in Compressible Flow." NACA TN 2337, April 1951.
33. Peters, C. E. and Phares, W. J. "An Integral Turbulent Kinetic Energy Analysis of Free Shear Flows." in Free Turbulent Shear Flows, Volume I, Conference Proceedings NASA SP 321, 1973, pp. 577-624.
34. Bradshaw, P. "Effects of Streamline Curvature on Turbulent Flow." AGARDograph AG169, August 1973.
35. Harsha, P. T. "Free Turbulent Mixing: A Critical Evaluation of Theory and Experiment." AEDC-TR-71-36 (AD718956), February 1971.
36. Mueller, T. J. "On Separation, Reattachment and Redevelopment of Turbulent Boundary Layers." Ph.D. Dissertation, University of Illinois, 1961.
37. Tani, I. "Experimental Investigation on Flow Separation Over a Step." Paper Presented at Symposium on Boundary Layer Research, Freiburg, Germany, August 26-29, 1957.
38. McDonald, H. "The Turbulent Supersonic Base Pressure Problem: A Comparison Between a Theory and Some Experimental Evidence." Report No. Ae 194, British Aircraft Corporation, April 1965.

39. Chapman, D. R., Wimbrow, W. R., and Kesler, R. H. "Experimental Investigation of Base Pressure on Blunt Trailing Edge Wings at Supersonic Velocities." NACA TN 2611, 1952.
40. Reda, D. C. and Page, R. H. "Supersonic Turbulent Flow Reattachment Downstream of a Two-Dimensional Back Step." AFOSR Scientific Report 69-1592 TR (Rutgers University RU-TR 125-MAE-F), May 1969.
41. Reid, J. and Hastings, R. C. "Experiments on the Axi-symmetric Flow over Afterbodies and Bases at $M = 2.0$." RAE Report Aero. 2628, October 1959.
42. Charters, A. C. and Turetsky, R. A. "Determination of Base Pressure from Free-Flight Data." BRL Report No. 653, March 1948.
43. Sirieix, M., Delery J., and Monnerie, B. "Etude Experimentale du Proche Sillage de Corps de Revolution en Ecoulement Supersonique." ONERA TP-608, 1968.
44. Donaldson, I. S. "The Effect of Sting Supports on the Base Pressure of a Blunt-Based Body in a Supersonic Stream." Aeronautical Quarterly, August 1955, pp. 221-229.
45. Badrinarayanan, M. A. "An Experimental Investigation of Base Flows at Supersonic Speeds." Journal of the Royal Aeronautical Society, Vol. 65, July 1961, pp. 475-482.
46. Rebuffet, R. "Effects de supports sur l'ecoulement a l'arriere d'un corps." AGARD RAPPORT 302, March 1959.
47. Seiling, W. R., Przirembel, C. E. G., and Page R. H. "Axisymmetric Turbulent Near-Wake Studies at Mach Four: Blunt and Hemispherical Bases." AFOSR Report No. 68-2465 (Rutgers University RU-TR 122-MAE-F), November, 1968.
48. Sinha, R. P, "Experimental and Theoretical Investigation of the Near Wake in an Axisymmetric Supersonic Flow with and without Base Injection." Ph.D. Dissertation, New York University, 1968.

APPENDIX A

COEFFICIENTS OF THE INTEGRAL EQUATIONS

The following parameters are defined:

$$y = (r - r_i)/b$$

$$r_s = r_i + b$$

$$r^a dr = ab^2 y dy + r_i^a b dy ; \quad a = 0 \text{ or } 1$$

$$S_{1g} = \frac{\partial}{\partial g} (\rho u)$$

$$S_{2g} = \frac{\partial}{\partial g} (\rho u^2)$$

$$S_{3g} = \frac{\partial}{\partial g} (\rho u C)$$

The jet regime coefficients (F, G, H, and I), where $g = p, r_i, b, K$, and x , are (the subscript c on p_c has been omitted for convenience):

$$F_1 = ab^2 \int_0^1 S_{1p} y dy + r_i^a b \int_0^1 S_{1p} dy + \frac{r_i^{a+1}}{(a+1)} \frac{d}{dp} (\rho_j u_j)$$

$$F_2 = ab^2 \int_0^1 S_{1r_i} y dy + r_i^a b \int_0^1 S_{1r_i} dy$$

$$F_3 = ab^2 \int_0^1 S_{1b} y dy + r_i^a b \int_0^1 S_{1b} dy$$

$$F_4 = ab^2 \int_0^1 S_{1K} y dy + r_i^a b \int_0^1 S_{1K} dy$$

$$F_5 = -ab^2 \int_0^1 S_{1x} y dy + r_i^a b \int_0^1 S_{1x} dy - \rho_s v_s r_s^a$$

$$G_1 = ab^2 \int_0^1 S_{2p} y dy + r_i^a b \int_0^1 S_{2p} dy + \frac{r_s^{a+1}}{(a+1)} + \frac{r_i^{a+1}}{(a+1)} \frac{d}{dp} (\rho_j u_j^2)$$

$$G_2 = ab^2 \int_0^1 S_{2r_i} y dy + r_i^a b \int_0^1 S_{2r_i} dy$$

$$G_3 = ab^2 \int_0^1 S_{2b} y dy + r_i^a b \int_0^1 S_{2b} dy$$

$$G_4 = \alpha b^2 \int_0^1 S_{2K} y dy + r_i^\alpha b \int_0^1 S_{2K} dy$$

$$G_5 = -\alpha b^2 \int_0^1 S_{2x} y dy - r_i^\alpha b \int_0^1 S_{2x} dy - \rho_s v_s u_s r_s^\alpha$$

$$H_1 = \alpha b^2 \int_0^{\frac{1}{2}} S_{2p} y dy + r_i^\alpha b \int_0^{\frac{1}{2}} S_{2p} dy - \alpha u_m b^2 \int_0^{\frac{1}{2}} S_{1p} y dy \\ - u_m r_i^\alpha b \int_0^{\frac{1}{2}} S_{1p} dy + \frac{r_m^{\alpha+1}}{(\alpha+1)} + \frac{r_i^{\alpha+1}}{(\alpha+1)} \frac{d}{dp} (\rho_j u_j^2) - u_m \frac{r_i^{\alpha+1}}{(\alpha+1)} \frac{d}{dp} (\rho_j u_j)$$

$$H_2 = \alpha b^2 \int_0^{\frac{1}{2}} S_{2r_i} y dy + r_i^\alpha b \int_0^{\frac{1}{2}} S_{2r_i} dy - \alpha u_m b^2 \int_0^{\frac{1}{2}} S_{1r_i} y dy - u_m r_i^\alpha b \int_0^{\frac{1}{2}} S_{1r_i} dy$$

$$H_3 = \alpha b^2 \int_0^{\frac{1}{2}} S_{2b} y dy + r_i^\alpha b \int_0^{\frac{1}{2}} S_{2b} dy - \alpha u_m b^2 \int_0^{\frac{1}{2}} S_{1b} y dy - u_m r_i^\alpha b \int_0^{\frac{1}{2}} S_{1b} dy$$

$$H_4 = \alpha b^2 \int_0^{\frac{1}{2}} S_{2K} y dy + r_i^\alpha b \int_0^{\frac{1}{2}} S_{2K} dy - \alpha u_m b^2 \int_0^{\frac{1}{2}} S_{1K} y dy - u_m r_i^\alpha b \int_0^{\frac{1}{2}} S_{1K} dy$$

$$H_5 = -\alpha b^2 \int_0^{\frac{1}{2}} S_{2x} y dy - r_i^\alpha b \int_0^{\frac{1}{2}} S_{2x} dy + \alpha u_m b^2 \int_0^{\frac{1}{2}} S_{1x} y dy \\ + u_m r_i^\alpha b \int_0^{\frac{1}{2}} S_{1x} dy + \tau_m r_m^\alpha$$

$$I_1 = \alpha b^2 \int_0^1 S_{3p} y dy + r_i^\alpha b \int_0^1 S_{3p} dy + \frac{r_i^{\alpha+1}}{(\alpha+1)} \frac{d}{dp} (\rho_j u_j)$$

$$I_2 = \alpha b^2 \int_0^1 S_{3r_i} y dy + r_i^\alpha b \int_0^1 S_{3r_i} dy$$

$$I_3 = \alpha b^2 \int_0^1 S_{3b} y dy + r_i^\alpha b \int_0^1 S_{3b} dy$$

$$I_4 = \alpha b^2 \int_0^1 S_{3K} y dy + r_i^\alpha b \int_0^1 S_{3K} dy$$

$$I_5 = -\alpha b^2 \int_0^1 S_{3x} y dy - r_i^\alpha b \int_0^1 S_{3x} dy$$

The wake regime coefficients (F, G, H, I, and J), where $g = u_c, r_i, b, K, C_c$ and x are:

$$F_1 = \alpha b^2 \int_0^1 S_{1u_c} y dy + r_i^{\alpha} b \int_0^1 S_{1u_c} dy + \frac{r_i^{\alpha+1}}{(\alpha+1)} \frac{\partial}{\partial u_c} (\rho_c u_c)$$

$$F_2 = \alpha b^2 \int_0^1 S_{1r_i} y dy + r_i^{\alpha} b \int_0^1 S_{1r_i} dy$$

$$F_3 = \alpha b^2 \int_0^1 S_{1b} y dy + r_i^{\alpha} b \int_0^1 S_{1b} dy$$

$$F_4 = \alpha b^2 \int_0^1 S_{1K} y dy + r_i^{\alpha} b \int_0^1 S_{1K} dy$$

$$F_5 = \alpha b^2 \int_0^1 S_{1C_c} y dy + r_i^{\alpha} b \int_0^1 S_{1C_c} dy + \frac{r_i^{\alpha+1}}{(\alpha+1)} \frac{\partial}{\partial C_c} (\rho_c u_c)$$

$$F_6 = -\alpha b^2 \int_0^1 S_{1x} y dy - r_i^{\alpha} b \int_0^1 S_{1x} dy - \rho_s v_s r_s^{\alpha}$$

$$G_1 = \alpha b^2 \int_0^1 S_{2u_c} y dy + r_i^{\alpha} b \int_0^1 S_{2u_c} dy + \frac{r_i^{\alpha+1}}{(\alpha+1)} \frac{\partial}{\partial u_c} (\rho_c u_c^2)$$

$$G_2 = \alpha b^2 \int_0^1 S_{2r_i} y dy + r_i^{\alpha} b \int_0^1 S_{2r_i} dy$$

$$G_3 = \alpha b^2 \int_0^1 S_{2b} y dy + r_i^{\alpha} b \int_0^1 S_{2b} dy$$

$$G_4 = \alpha b^2 \int_0^1 S_{2K} y dy + r_i^{\alpha} b \int_0^1 S_{2K} dy$$

$$G_5 = \alpha b^2 \int_0^1 S_{2C_c} y dy + r_i^{\alpha} b \int_0^1 S_{2C_c} dy + \frac{r_i^{\alpha+1}}{(\alpha+1)} \frac{\partial}{\partial C_c} (\rho_c u_c^2)$$

$$G_6 = -\alpha b^2 \int_0^1 S_{2x} y dy - r_i^{\alpha} b \int_0^1 S_{2x} dy - \rho_s u_s v_s r_s^{\alpha}$$

$$H_1 = \alpha b^2 \int_0^{\frac{1}{2}} S_{2u_c} y dy + r_i^{\alpha} b \int_0^{\frac{1}{2}} S_{2u_c} dy - u_m \alpha b^2 \int_0^{\frac{1}{2}} S_{1u_c} y dy - u_m r_i^{\alpha} b \int_0^{\frac{1}{2}} S_{1u_c} dy$$

$$+ \frac{r_i^{\alpha+1}}{(\alpha+1)} \frac{\partial}{\partial u_c} (\rho_c u_c^2) - u_m \frac{r_i^{\alpha+1}}{(\alpha+1)} \frac{\partial}{\partial u_c} (\rho_c u_c)$$

$$H_2 = \alpha b^2 \int_0^{\frac{1}{2}} S_{2r_i} y dy + r_i^{\alpha} b \int_0^{\frac{1}{2}} S_{2r_i} dy - u_m \alpha b^2 \int_0^{\frac{1}{2}} S_{1r_i} y dy - u_m r_i^{\alpha} b \int_0^{\frac{1}{2}} S_{1r_i} dy$$

$$H_3 = \alpha b^2 \int_0^{\frac{1}{2}} S_{2b} y dy + r_i^{\alpha} b \int_0^{\frac{1}{2}} S_{2b} dy - u_m \alpha b^2 \int_0^{\frac{1}{2}} S_{1b} y dy - u_m r_i^{\alpha} b \int_0^{\frac{1}{2}} S_{1b} dy$$

$$H_4 = \alpha b^2 \int_0^{\frac{1}{2}} S_{2K} y dy + r_i^{\alpha} b \int_0^{\frac{1}{2}} S_{2K} dy - u_m \alpha b^2 \int_0^{\frac{1}{2}} S_{1K} y dy - u_m r_i^{\alpha} b \int_0^{\frac{1}{2}} S_{1K} dy$$

$$H_5 = \alpha b^2 \int_0^{\frac{1}{2}} S_{2C_c} y dy + r_i^{\alpha} b \int_0^{\frac{1}{2}} S_{2C_c} dy - u_m \alpha b^2 \int_0^{\frac{1}{2}} S_{1C_c} y dy - u_m r_i^{\alpha} b \int_0^{\frac{1}{2}} S_{1C_c} dy \\ + \frac{r_i^{\alpha+1}}{(\alpha+1)} \frac{\partial}{\partial C_c} (\rho_c u_c^2) - u_m \frac{r_i^{\alpha+1}}{(\alpha+1)} \frac{\partial}{\partial C_c} (\rho_c u_c)$$

$$H_6 = -\alpha b^2 \int_0^{\frac{1}{2}} S_{2x} y dy - r_i^{\alpha} b \int_0^{\frac{1}{2}} S_{2x} dy + u_m \alpha b^2 \int_0^{\frac{1}{2}} S_{1x} y dy \\ + u_m r_i^{\alpha} b \int_0^{\frac{1}{2}} S_{1x} dy + \tau_m r_m^{\alpha}$$

$$I_1 = \alpha b^2 \int_0^1 S_{3u_c} y dy + r_i^{\alpha} b \int_0^1 S_{3u_c} dy + \frac{r_i^{\alpha+1}}{(\alpha+1)} \frac{\partial}{\partial u_c} (\rho_c u_c C_c)$$

$$I_2 = \alpha b^2 \int_0^1 S_{3r_i} y dy + r_i^{\alpha} b \int_0^1 S_{3r_i} dy$$

$$I_3 = \alpha b^2 \int_0^1 S_{3b} y dy + r_i^{\alpha} b \int_0^1 S_{3b} dy$$

$$I_4 = \alpha b^2 \int_0^1 S_{3K} y dy + r_i^{\alpha} b \int_0^1 S_{3K} dy$$

$$I_5 = \alpha b^2 \int_0^1 S_{3C_c} y dy + r_i^{\alpha} b \int_0^1 S_{3C_c} dy + \frac{r_i^{\alpha+1}}{(\alpha+1)} \frac{\partial}{\partial C_c} (\rho_c u_c C_c)$$

$$I_6 = -\alpha b^2 \int_0^1 S_{3x} y dy - r_i^{\alpha} b \int_0^1 S_{3x} dy$$

$$J_1 = \alpha b^2 \int_0^{\frac{1}{2}} S_{3u_c} y dy + r_i^{\alpha} b \int_0^{\frac{1}{2}} S_{3u_c} dy - C_m \alpha b^2 \int_0^{\frac{1}{2}} S_{1u_c} y dy - C_m r_i^{\alpha} b \int_0^{\frac{1}{2}} S_{1u_c} dy \\ + \frac{r_i^{\alpha+1}}{(\alpha+1)} \frac{\partial}{\partial u_c} (\rho_c u_c C_c) - C_m \frac{r_i^{\alpha+1}}{(\alpha+1)} \frac{\partial}{\partial u_c} (\rho_c u_c)$$

$$J_2 = \alpha b^2 \int_0^{\frac{1}{2}} S_{3r_i} y dy + r_i^{\alpha} b \int_0^{\frac{1}{2}} S_{3r_i} dy - C_m \alpha b^2 \int_0^{\frac{1}{2}} S_{1r_i} y dy - C_m r_i^{\alpha} b \int_0^{\frac{1}{2}} S_{1r_i} dy$$

$$J_3 = \alpha b^2 \int_0^{\frac{1}{2}} S_{3b} y dy + r_i^\alpha b \int_0^{\frac{1}{2}} S_{3b} dy - C_m \alpha b^2 \int_0^{\frac{1}{2}} S_{1b} y dy - C_m r_i^\alpha b \int_0^{\frac{1}{2}} S_{1b} dy$$

$$J_4 = \alpha b^2 \int_0^{\frac{1}{2}} S_{3K} y dy + r_i^\alpha b \int_0^{\frac{1}{2}} S_{3K} dy - C_m \alpha b^2 \int_0^{\frac{1}{2}} S_{1K} y dy - C_m r_i^\alpha b \int_0^{\frac{1}{2}} S_{1K} dy$$

$$J_5 = \alpha b^2 \int_0^{\frac{1}{2}} S_{3C_c} y dy + r_i^\alpha b \int_0^{\frac{1}{2}} S_{3C_c} dy - C_m \alpha b^2 \int_0^{\frac{1}{2}} S_{1C_c} y dy - C_m r_i^\alpha b \int_0^{\frac{1}{2}} S_{1C_c} dy \\ + \frac{r_i^{\alpha+1}}{(\alpha+1)} \frac{\partial}{\partial C_c} (\rho_c u_c C_c) - C_m \frac{r_i^{\alpha+1}}{(\alpha+1)} \frac{\partial}{\partial C_c} (\rho_c u_c)$$

$$J_6 = -\alpha b^2 \int_0^{\frac{1}{2}} S_{3x} y dy - r_i^\alpha b \int_0^{\frac{1}{2}} S_{3x} dy + C_m \alpha b^2 \int_0^{\frac{1}{2}} S_{1x} y dy + C_m r_i^\alpha b \int_0^{\frac{1}{2}} S_{1x} dy \\ + q_m r_m^\alpha$$

In the fully developed regime define

$$y = r/b$$

$$r_s = b$$

$$r^\alpha dr = b(b y)^\alpha dy$$

The fully developed regime coefficients (F, G, H, I, and J), where $g = p, u_c, b, K, C_c$ and x are:

$$F_1 = b b^\alpha \int_0^1 S_{1p} y^\alpha dy$$

$$F_2 = b b^\alpha \int_0^1 S_{1u_c} y^\alpha dy$$

$$F_3 = b b^\alpha \int_0^1 S_{1b} y^\alpha dy$$

$$F_4 = b b^\alpha \int_0^1 S_{1K} y^\alpha dy$$

$$F_5 = b b^\alpha \int_0^1 S_{1C_c} y^\alpha dy$$

$$F_6 = b b^\alpha \int_0^1 S_{1x} y^\alpha dy - \rho_s v_s r_s^\alpha$$

$$G_1 = bb^a \int_0^1 S_{2p} y^a dy + \frac{r_s^{a+1}}{(a+1)}$$

$$G_2 = bb^a \int_0^1 S_{2u_c} y^a dy$$

$$G_3 = bb^a \int_0^1 S_{2b} y^a dy$$

$$G_4 = bb^a \int_0^1 S_{2K} y^a dy$$

$$G_5 = bb^a \int_0^1 S_{2C_c} y^a dy$$

$$G_6 = - bb^a \int_0^1 S_{2x} y^a dy - \rho_s v_s u_s r_s^a$$

$$H_1 = bb^a \int_0^{1/2} S_{2p} y^a dy - u_m bb^a \int_0^{1/2} S_{1p} y^a dy + \frac{r_m^{a+1}}{(a+1)}$$

$$H_2 = bb^a \int_0^{1/2} S_{2u_c} y^a dy - u_m bb^a \int_0^{1/2} S_{1u_c} y^a dy$$

$$H_3 = bb^a \int_0^{1/2} S_{2b} y^a dy - u_m bb^a \int_0^{1/2} S_{1b} y^a dy$$

$$H_4 = bb^a \int_0^{1/2} S_{2K} y^a dy - u_m bb^a \int_0^{1/2} S_{1K} y^a dy$$

$$H_5 = bb^a \int_0^{1/2} S_{2C_c} y^a dy - u_m bb^a \int_0^{1/2} S_{1C_c} y^a dy$$

$$H_6 = - bb^a \int_0^{1/2} S_{2x} y^a dy + u_m bb^a \int_0^{1/2} S_{1x} y^a dy + \tau_m r_m^a$$

$$I_1 = bb^a \int_0^1 S_{3p} y^a dy$$

$$I_2 = bb^a \int_0^1 S_{3u_c} y^a dy$$

$$I_3 = bb^a \int_0^1 S_{3b} y^a dy$$

$$I_4 = bb^a \int_0^1 S_{3K} y^a dy$$

$$I_5 = bb^a \int_0^1 S_{3C_c} y^a dy$$

$$I_6 = - bb^a \int_0^1 S_{3x} y^a dy$$

$$J_1 = bb^a \int_0^{1/2} S_{3p} y^a dy - C_m bb^a \int_0^{1/2} S_{1p} y^a dy$$

$$J_2 = bb^a \int_0^{1/2} S_{3u_c} y^a dy - C_m bb^a \int_0^{1/2} S_{1u_c} y^a dy$$

$$J_3 = bb^a \int_0^{1/2} S_{3b} y^a dy - C_m bb^a \int_0^{1/2} S_{1b} y^a dy$$

$$J_4 = bb^a \int_0^{1/2} S_{3K} y^a dy - C_m bb^a \int_0^{1/2} S_{1K} y^a dy$$

$$J_5 = bb^a \int_0^{1/2} S_{3C_c} y^a dy - C_m bb^a \int_0^{1/2} S_{1C_c} y^a dy$$

$$J_6 = - bb^a \int_0^{1/2} S_{3x} y^a dy + C_m bb^a \int_0^{1/2} S_{1x} y^a dy + q_m r_m^a$$

NOMENCLATURE

b	Shear layer thickness
c_p	Specific heat at constant pressure
C	Element fraction of bleed gas
F, G, H, I, J	Coefficients in system of ordinary differential equations
g	Generalized variable (Appendix A)
h	Base height in planar flow
K	Parameter in species profile equation
M	Mach number
n	Boundary-layer profile exponent
N	Generalized coefficient in system of ordinary differential equations
p	Static pressure
p_b	Base pressure
p_o	Total pressure
p_o'	Pitot pressure
\bar{P}	Pressure gradient parameter
q	Turbulent species flux
r	Lateral coordinate
r_b	Base radius
r_i	Lateral distance from centerline to inner edge of shear layer
r_s	Lateral distance from centerline to outer edge of shear layer
R	Gas constant
RSP	Rear stagnation point

Re_θ	Momentum thickness Reynolds number
Re_T	Turbulent Reynolds number
S	Generalized integrand (Appendix A)
T_o	Total temperature
u	Axial velocity component
v	Lateral velocity component
x	Axial coordinate
Δx	Integration step size
y	Distance from wall in initial boundary layer; dimensionless mixing zone coordinate (Appendix A)
a	Geometric parameter (one for axisymmetric flow, zero for planar flow)
γ	Ratio of specific heats
δ	Initial boundary-layer thickness
δ_p	Distance at beginning of recompression between centerline and streamline which originates at outer edge of initial boundary layer
θ	Momentum thickness of initial boundary layer
ρ	Density
τ	Turbulent shear stress

SUBSCRIPTS

1	Conditions before base expansion
a	Outer free stream
c	Centerline
d	Conditions on dividing streamline
j	Conditions in base bleed flow

m	Conditions at middle of shear layer
p	Conditions at beginning of recompression
r	Conditions at rear stagnation point